Processive phosphorylation of ERK MAP kinase in mammalian cells.

AUTHOR(S):

Aoki, Kazuhiro; Yamada, Masashi; Kunida, Katsuyuki; Yasuda, Shuhei; Matsuda, Michiyuki

CITATION:

Aoki, Kazuhiro ...[et al]. Processive phosphorylation of ERK MAP kinase in mammalian cells.. Proceedings of the National Academy of Sciences of the United States of America 2011, 108(31): 12675-12680

ISSUE DATE:

2011-07-18

URL:

http://hdl.handle.net/2433/143060

Title page

Classification: Biological Sciences, Biochemistry, Cell Biology

Title

Processive phosphorylation of ERK MAP kinase in mammalian cells

Kazuhiro Aoki,[a,b,1,*] Masashi Yamada,[c,1] Katsuyuki Kunida,[c] Shuhei Yasuda,[a] and Michiyuki Matsuda[a,c]

[a] Laboratory of Bioimaging and Cell Signaling, Graduate School of Biostudies, Kyoto University, Sakyo-ku, Kyoto 606-8501, Japan,

[b] PREST, Japan Science and Technology Agency (JST), 4-1-8 Honcho Kawaguchi, Saitama 332-0012, Japan

[c] Department of Pathology and Biology of Diseases, Graduate School of Medicine, Kyoto University, Sakyo-ku, Kyoto 606-8501, Japan

[1] These authors contributed equally to this work.

[*] Correspondence: k-aoki@lif.kyoto-u.ac.jp

Keywords: ERK, simulation, processive model, distributive model

Abstract

The mitogen-activated protein (MAP) kinase pathway is comprised of a three-tiered kinase cascade. The distributive kinetic mechanism of two-site MAP kinase phosphorylation inherently generates a non-linear switch-like response. However, a linear graded response of MAP kinase has also been observed in mammalian cells, and its molecular mechanism remains unclear. To dissect these input-output behaviors, we quantitatively measured the kinetic parameters involved in the MEK-ERK MAP kinase signaling module in HeLa cells. Using a numerical analysis based on experimentally determined parameters, we predicted *in silico* and validated *in vivo* that ERK is processively phosphorylated in HeLa cells. Finally, we identified molecular crowding as a critical factor that converts distributive phosphorylation into processive phosphorylation. We proposed the term *quasi-processive phosphorylation* to describe this mode of ERK phosphorylation that is operated under the physiological condition of molecular crowding. The generality of this phenomenon may provide a new paradigm for a diverse set of biochemical reactions including multiple posttranslational modifications.

¥body

Introduction

Mitogen-activated protein (MAP) kinase cascades are evolutionarily conserved signaling pathways that are involved in the control of physiological and pathological cellular processes including cell proliferation, survival, differentiation, apoptosis, and tumorigenesis (1-4). Each MAP kinase pathway contains a three-tiered kinase cascade consisting of a MAP kinase kinase kinase, a MAP kinase kinase, and the MAP kinase, which are sequentially activated in this order. MAP kinases, which are activated by dual phosphorylation of conserved threonine and tyrosine residues within the activation loop, phosphorylate their targets on serine or threonine residues (1, 3, 5). Five distinct groups of MAP kinases have been characterized in mammals. Among them, the most studied is the Raf/MEK/ERK MAP kinase cascade (hereafter called the ERK MAP kinase cascade), which is activated by mitogenic ligands such as growth factors, cytokines, and phorbol esters.

Ferrell and coworkers found that in *Xenopus* oocytes the ERK MAP kinase pathway responds to increasing levels of progesterone in an all-or-none or “switch-like” manner, in which individual cells in the population exhibit either “on” or “off” status (6, 7). This property of ERK MAP kinase system befits to determine all-or-none irreversible responses including cell-cycle progression, neuronal differentiation, and T cell selection (6-10). The switch-like responses can arise from both positive feedback via protein synthesis and dual phosphorylation steps of the MAP kinase, which is called the “distributive phosphorylation model” (11-15) (Fig. 1A). The distributive model of ERK phosphorylation results in an increase in the cooperativity of this system, and consequently contributes to a switch-like input-output response.

In different cellular contexts, however, the ERK MAP kinase cascade exhibits “graded” response, in which all cells in the population uniformly gain their signal output proportionally in response to the level of input stimulus. This input-output response is observed in the pheromone-stimulated *S. cerevisiae* (16-18) and growth factor stimulated-HeLa cells and fibroblasts (19, 20). These graded responses can suit the physiological property of signaling, including the reversibility and the activation by different inputs with a wide range of threshold doses (18). However, MAP kinase cascades should inherently induce the switch-like response behavior due to the three-tiered enzyme cascade. To answer this question, it has been theoretically proposed that scaffold proteins might convert the switch-like response into the graded response (21). Here, the scaffold protein holds MAP kinase kinase and MAP kinase, thereby inducing dual phosphorylation at a single collision, which is called the “processive phosphorylation model” (11, 21-25). However, it is not known whether the scaffold proteins in mammals contribute to the processive phosphorylation of MAP kinase (10). Hence, the mechanism by which MAP kinase activity adopts a graded response remains unclear in mammalian cells.

In this study, we demonstrate for the first time that ERK is phosphorylated in a processive manner by employing quantitative simulation model of the ERK MAP kinase cascade. Furthermore, a condition that mimics physiological molecular crowding has been shown to convert the mode of ERK phosphorylation from distributive to processive. Under this condition, MEK and ERK do not form a stable complex as proposed in the processive phosphorylation model. Therefore, we propose that ERK is phosphorylated in a “quasi-processive” manner under the physiological condition of molecular crowding.

Results

Kinetic parameters that determine the dynamics of the MEK-ERK signaling module

Our goal is to comprehend the systems behavior of the MEK-ERK signaling module. To this end, we attempted to determine most, if not all, of the kinetic parameters required for the kinetic simulation model, using HeLa cells as a model system. The model requires four classes of parameters: protein concentrations, association/dissociation rates, nuclear import/export rates, and phosphorylation/dephosphorylation rates. We experimentally determined approximately 30 parameters (SI Appendix, Fig. S1-7 and Tables S1 and S2). Notably, this study focused on the phosphorylation kinetics of the MEK-ERK module in the early phase of the signaling event. Thus, we neglected the role of ERK-induced gene expression of negative regulators such as dual specificity phosphatases (DUSPs), which shape the dynamics of intracellular signaling starting from 30 min after ligand addition (26).

In vitro phosphorylation rates of ERK measured by Phos-tag gel electrophoresis

All parameters used in this study are determined in living HeLa cells except for the phosphorylation rates of ERK, which was determined as follows. MEK activates ERK by phosphorylating two critical amino acid residues within the activation loop, threonine and tyrosine; therefore, we quantified four phospho-isoforms of ERK, non-phosphorylated ERK (np-ERK), tyrosine mono-phosphorylated ERK (pY-ERK), threonine mono-phosphorylated ERK (pT-ERK), and bis-phosphorylated ERK (pTpY-ERK) by Phos-tag western blotting (27). Phos-tag is a phosphorylated amino acid chelator. Because the electrophoretic mobility of phosphorylated proteins is significantly reduced in separation gels containing Phos-tag, the

fractions of non-phosphorylated and phosphorylated proteins can be visualized quantitatively. Notably, the effect of Phos-tag on the electrophoretic mobility varies among phospho-proteins, demanding a preliminary experiment of the identification of each phospho-protein by immunoblotting with specific antibodies (SI Appendix, Fig. S4). We found that the order of electrophoretic mobility in the Phos-tag gel was, from the slowest to fastest, pY-ERK, pTpY-ERK, pT-ERK, and np-ERK. This order was also confirmed with phosphatase inhibitors. Treatment with the phospho-tyrosine phosphatase inhibitor bpV, and the phospho-serine/threonine phosphatase inhibitor Calyculin A, increased the intensity of the pY-ERK and pT-ERK bands, respectively (SI Appendix, Fig. S6).

The rates of ERK phosphorylation by MEK were first determined *in vitro* using a kinase-dead mutant of ERK2 (ERK2-KR) and constitutively active mutant of MEK1 (MEK1-SDSE). As previously demonstrated (11), pY-ERK was initially accumulated, followed by pTpY-ERK (Fig. 1B and 1C). pT-ERK could not be detected under this condition. Importantly, the amount of the intermediate product, pY-ERK, exceeded that of the enzyme, MEK1-SDSE (3.0×10^{-7} M in Fig. 1C), indicating that ERK was phosphorylated by a manner consistent with the distributive phosphorylation model *in vitro* (11). In this way, we obtained the first and second reaction rates with linear assumption (k_{cat}/K_m) of 3.9×10^4 [/M/sec] and 2.1×10^4 [/M/sec], respectively (SI Appendix, Fig. S5 and Table S2). The reason why pT-ERK was not detected may be because the first step of the reactions from np-ERK to pT-ERK is markedly slower than the second step from pT-ERK to pTpY-ERK *in vitro*. Therefore, the phosphorylation reaction rate (k_{cat}/K_m) from pT-ERK to pTpY-ERK was examined *in vitro* using pT-ERK as a substrate, and was found to be 2.0×10^4 [/M/sec] (SI Appendix, Table S2). Thus, pT-ERK production from np-ERK could be ignored at least in the phosphorylation reactions (SI Appendix, Fig. S5G).

Validation of the distributive phosphorylation model

Based on these parameters determined experimentally (SI Appendix, Tables S1 and S2), we built a distributive phosphorylation model of the MEK-ERK signaling module (Fig. 2A and SI Appendix, Fig. S8A), and numerically solved the ERK phosphorylation (Fig. 2B and 2C). The input signal, i.e., the turnover rate of MEK phosphorylation by cRaf, was initially set to 1.0×10^6 [/M/sec] to reproduce the experimental data, and was varied with a broad range (SI Appendix, Fig. S9). Upon stimulation *in silico*, pY-ERK was steeply increased, followed by a gradual increase in pTpY-ERK and pT-ERK (Fig. 2B). pY-ERK was predominant over pTpY-ERK in low input strength, and vice versa for high input strength at 10 min after stimulation (Fig. 2C). These data were consistent with the distributive phosphorylation model demonstrated *in vitro* (Fig. 1) and in *Xenopus* oocytes (6, 11).

We next examined whether the phosphorylation of ERK2 in HeLa cells follows the distributive model. Against the prediction *in silico*, the increase in pY-ERK2 did not precede to, but rather accompanied the increase in pTpY-ERK2 upon EGF stimulation (Fig. 2D and 2E). Furthermore, pY-ERK2 increased in a dose-dependent manner as the EGF input increased (Fig. 2F and 2G), but did not increase in a bell-shaped manner as predicted *in silico* (Fig. 2C). Of note, we could not detect the endogenous pT-ERK2 quantitatively due to the low abundance and to the signals of co-migrating pY-ERK1.

Prediction of a processive phosphorylation model *in silico*

Because we determined all parameters in the cells except for the phosphorylation reaction rates, which were obtained *in vitro*, we speculated that the discrepancy between the experimental and

in silico data of the MEK-induced ERK phosphorylation might have arisen from parameters related to the phosphorylation rates of ERK. Hence, we built a processive model by changing one reaction pathway of the distributive model (Fig. 3A and SI Appendix, Fig. S8B, Tables S1 and S2). Here, activated MEK does not dissociate from pY-ERK but processively phosphorylates threonine of pY-ERK to generate pTpY-ERK. Therefore, this model contains two species of pY-ERK, i.e. pY-ERK in complex with MEK and pY-ERK generated by the dephosphorylation of pTpY-ERK.

With this processive model, the experimental observation (Fig. 2D-2G) was reproduced successfully (Fig. 3B, 3C and SI Appendix, Fig. S9). Namely, the increase in pY-ERK paralleled the increase in pTpY-ERK both in the time course analysis and the input-output response analysis. These results implied that ERK is processively phosphorylated by MEK.

Experimental validation of the processive model 1: pY-ERK dynamics

By employing computer-assisted kinetic simulation, we designed an experimental condition that distinguishes between the distributive model and the processive model. When cells are stimulated in the presence of phosphatase inhibitors, pY-ERK will be increased in the distributive model (Fig. 4A, green lines, and SI Appendix, Fig. S10A) and decreased in the processive model (Fig. 4B, green lines, and SI Appendix, Fig. S10B). This is because pY-ERK is generated primarily as the intermediate phosphorylation product in the distributive model, whereas in the processive model pY-ERK is produced by the dephosphorylation of pTpY-ERK. For the execution of the designed experiment, HeLa cells were stimulated with EGF in the absence or presence of inhibitors for tyrosine- and serine/threonine-phosphatase, bpV and Calyculin A, respectively. As expected in the processive model, phosphatase inhibitors substantially reduced

the accumulation of pY-ERK, arguing for the processive phosphorylation model (Fig. 4C and 4D).

Experimental validation of the processive model 2: Input-output response

Previous studies supported the distributive phosphorylation model primarily because it explains the non-linear switch-like response of MAP kinase upon stimulation. Therefore, to understand the contribution of the MEK-ERK signaling module to the switch-like response of ERK to EGF, we examined the input-output behavior of ERK phosphorylation in our experimental conditions. We quantified the amount of pTpY-ERK1/2 in individual cells by immuno-staining with anti-pTpY-ERK1/2 antibody. As reported previously in HeLa cells and fibroblasts stimulated with EGF and TPA, respectively (19, 20), this approach could provide quantitative relationship between the input signal and output response (Fig. 5A and 5B). The Hill coefficient obtained by this method was 2.09 (Fig. 5B). Next, we confirmed this observation by western blotting, which also demonstrated a mild non-linear cooperativity, having 1.91 Hill coefficient (Fig. 5C). However, when we examined the correlation of the fraction of active MEK with the fraction of pTpY-ERK, we observed almost linear input-output response of ERK, having 1.18 Hill coefficient (Fig. 5D). Importantly, this Hill coefficient value determined experimentally was nearly identical to the Hill coefficient calculated at 1.19 by the processive model (Fig. 5F), but significantly smaller than the Hill coefficient calculated at 1.61 by the distributive model (Fig. 5E). Notably, the Hill coefficients might be slightly overestimated because they were calculated at the time point before reaching plateau. Nevertheless, these results strongly supported the processive model, which should exhibit linear input-output response.

Numerical validation of the processive model

To examine which of the distributive and processive models is the plausible mechanism to account for the observed data (Fig. 2E and Fig. 4D), we calculated residual sum of squares (RSS) values, Akaike information criterion (AIC) values, and Hill coefficients for both models after parameter fitting (28) (Fig. S11). This in silico validation was performed under three conditions of different numbers of variables. Condition 1: all phosphorylation rates were multiplied by a common constant value, which was optimized to fit the experimental data. Condition 2: the phosphorylation rates were individually fitted to the experimental data. Condition 3: in addition to the phosphorylation rates, the dephosphorylation rates were also fitted individually to the experimental data. In all conditions, experimentally-determined parameters were used as the initial values for the fitting. In Conditions 1 and 2, the processive model was more plausible than the distributive model because the AIC of the former model was smaller than the AIC of the latter model. Although both distributive and processive models exhibited the lowest RSS in Condition 3, the AIC values were higher than those in the other conditions, which indicated over-fitting in Condition 3. Importantly, the Hill coefficients calculated by the processive model were closer to the experimental value than the Hill coefficients calculated by the distributive model (Fig. 5F). Taken together, these analyses strongly argued that ERK is processively phosphorylated by MEK in HeLa cells.

Molecular crowding as a determinant for processive phosphorylation

What kind of factor(s) is a critical determinant for changing the distributive nature of ERK phosphorylation into the processive one in the cells? A critical difference between the environment *in vitro* and that within cells is the effect of molecular crowding (29, 30). To

evaluate the effect of molecular crowding, we examined whether or not ERK is phosphorylated in a processive manner in diluted cytoplasmic cell extract. Similarly to the results of *in vitro* ERK phosphorylation, ERK is phosphorylated in a distributive manner in the cytoplasmic extract, which was manifested by the initial accumulation of pY-ERK (SI Appendix, Fig. S12). Conversely, we mimicked the physiological molecular crowding by adding 15% (wt/vol) polyethylene glycol (PEG) to *in vitro* kinase reaction solution as a crowder (31) (Fig. 6A and 6B). The addition of PEG reduced the production rate of pY-ERK without changing the net production rate of pTpY-ERK, indicating an increase in the "processivity" of ERK phosphorylation (Fig. 6C and 6D). Lastly, we built a partial processive model by combining the distributive and processive models and fitted it to the experimental data (Fig. 6E). For this we introduced two additional parameters: Processivity, p, as the probability of pTpY-ERK production in the processive manner, and crowding factor, c, as the effect of the crowder or viscosity on the net reaction rates. By the fitting we found that the presence of 15% PEG increased in the processivity of ERK phosphorylation of 47%, and decreased the reaction rates to 27% by viscosity (Fig. 6C and 6D). Of note, the amount of pY-ERK at the zenith exceeded the net amount of MEK (Fig. 6D, dashed line), indicating that pY-ERK was not accumulated due to the sequestration by MEK binding. Thus, the molecular crowding within the cells could convert the distributive phosphorylation in vitro to the processive phosphorylation as seen in the cells.

Discussion

In this study, we have demonstrated for the first time that the amino acid residues in the activation loop of ERK, threonine and tyrosine, are processively phosphorylated in HeLa cells, and have identified molecular crowding as one possible factor in determining whether the mode of phosphorylation will be distributive or processive. The term “processive phosphorylation” is used to describe reactions in which the substrate-enzyme complex is stable during the first and second phosphorylation reactions, which is not the case for the phosphorylation of ERK (Fig. 6D). We therefore proposed the term “quasi-processive phosphorylation” to describe two sequential phosphorylation reactions that are controlled by molecular crowding (Fig. 6F). In this model, MEK first phosphorylates ERK at the tyrosine residue and dissociates from the product, pY-ERK. Under the physiological conditions within cells, the diffusions of both MEK and pY-ERK are considerably restricted by the molecular crowding effect; therefore, MEK rebinds to and phosphorylates pY-ERK with high probability. Consequently, MEK phosphorylates ERK in a processive manner. Another MAP kinase, p38, also exhibited typical hallmarks of the processive phosphorylation (SI Appendix, Fig. S13), indicating the generality of the quasi-processive phosphorylation of MAP kinase within cells. In contrast to the phosphorylation step, this quasi-processive phosphorylation model could not be applicable to the dephosphorylation step of pTpY-ERK, because the premise of quasi-processive phosphorylation is sequential reactions operated by the identical enzyme. The dephosphorylation reactions of phospho-threonine and phospho-tyrosine were mediated probably by different classes of phosphatase at least in our experimental conditions (SI Appendix, Fig. S6).

The quasi-processive phosphorylation is critically different from the previously proposed processive phosphorylation model, in which scaffold proteins anchor MEK and ERK in order to cause sequential phosphorylation reactions by a single collision (21). The scaffold proteins are

known to regulate assembly of two or more components of signaling pathways in many signaling cascades (21-25). As far as we have examined, however, none of the scaffold proteins for MEK and ERK contributed significantly to cause the processivity of ERK phosphorylation (SI Appendix, Fig. S14), consistent with the previous study on KSR (10).Therefore, at this moment, we failed to obtain any evidence that scaffold proteins cause processive phosphorylation in mammalian cells. Importantly, Takahashi and Pryciak have concluded that sole expression of Ste5 scaffold did not induce linear response of MAP kinase phosphorylation in yeast, and instead the recruitment of the scaffold to the plasma membrane resulted in linear response of MAP kinase phosphorylation (18). This seems to fit very well with our findings, in that the effect of Ste5 could be due to molecular crowding or confinement, rather than scaffolding *per se*. Recently, Takahashi *et al*, demonstrated by particle simulation that rapid rebinding of enzyme molecules to the substrate after modification of the first site can turn a distributive model into a processive model (32). They have predicted that molecular crowding will make enzyme-substrate rebindings more likely due to subdiffusion, strongly providing the theoretical basis of our findings.

It has been suggested that the high cooperativity of *Xenopus* oocytes in reaction to progesterone stimulation is at least partly accomplished by the distributive phosphorylation of ERK (6, 7). Some degree of molecular crowding probably exists in *Xenopus* oocytes, indicating an important point of disagreement between these previous studies and our present findings. However, it should be noted that the phosphorylation dynamics of ERK phospho-isoforms has only been investigated *in vitro*, and has never been investigated experimentally in *Xenopus* oocytes or cells. Therefore, it is possible that ERK is processively phosphorylated in *Xenopus* oocytes as in HeLa cells. There may exist non-linear reactions in the signaling pathway upstream

of MEK, e.g., receptor phosphorylation or Mos activation, in *Xenopus* oocytes. Actually, the input-output relationship between EGF concentration and pTpY-ERK demonstrated higher cooperativity; namely, the Hill coefficient was almost two (Fig. 5A-C). In contrast, the Hill coefficient for active MEK and pTpY-ERK phosphorylation was approximately one, implying the presence of a non-linear reaction(s) in the signaling cascade upstream of MEK. Consistent with this assumption, it has been reported that EGFR phosphorylation responded in a highly amplified and switch-like manner by coupling EGFR activation and PTP inhibition (33).

As has been described in this study, the discrepancy between the data acquired from the cells and the data predicted by the kinetic simulation model led us to the finding that ERK is processively phosphorylated within cells. Therefore, our results underscore the importance of simulation models based on experimentally determined kinetic parameters. Another important message from this study is that, in some cases, the physiological condition of molecular crowding significantly affected the mode of phosphorylation. Recent proteomic data demonstrates that proteins in a eukaryotic cell harbor multiple phosphorylation sites, each of which regulates different functions of their proteins (24). Therefore, molecular crowding, which is ubiquitous in biological systems, introduces additional complexity in their regulation. Thus, the finding that molecular crowding changes the mode of successive reactions to a processive type provides a new paradigm for a diverse set of biochemical reactions.

Materials and Methods

Plasmids, cells, reagents and antibodies

The plasmids used here were constructed according to the standard methods. Cells, reagents and antibodies are detailed in SI Appendix.

Purification of recombinant proteins, cytoplasm extract and *in vitro* kinase assay

Details of purification of recombinant proteins, cytoplasmic extract and *in vitro* kinase assay are provided in SI Appendix.

Phos-tag polyacrylamide gel electrophoresis

Phos-tag polyacrylamide gel electrophoresis was performed essentially as described previously (27). For Phos-tag western blottings of ERK and p38, 5.0×10^{-5} and 1.5×10^{-4} M Phos-tag and 1.0×10^{-4} and 3.0×10^{-4} M $MnCl_2$ were added to conventional SDS-polyacrylamide separation gels according to the manufacturer's protocol, respectively. Proteins were detected by using an Odyssey Infrared Imaging System (LI-COR).

Imaging

Live cell imaging was performed essentially as described (34).

Kinetic modeling and numerical simulation

Numerical simulation and parameter search were implemented by MATLAB software with ode23 and fminsearch function, respectively. The details are described in SI Appendix.

Immunostaining

Details of pTpY-ERK immunostaining are provided in SI Appendix.

Data analysis

For the determination of kinetic parameters, curve fitting were performed by the solver function

of Microsoft excel (Microsoft, WA).

Acknowledgments

We thank M. White, B. Neel, A. Miyawaki, T. Akagi, F. Ishikawa and J. Miyazaki for the plasmids. A. Nishiyama-Abe, R. Sakai, Y. Kasakawa, and N. Nonaka are also to be thanked for their technical assistance. We are grateful to the members of the Matsuda Laboratory for their helpful discussions. KA and MM were supported by Research Program of Innovative Cell Biology by Innovative Technology (Cell Innovation) from the Ministry of Education, Culture, Sports, and Science, Japan. KA was supported by the JST PRESTO program. MY and KK were supported by the Global COE Program "Center for Frontier Medicine" initiated by the Ministry of Education, Culture, Sports, Science, and Technology, Japan.

References

1. Qi M & Elion EA (2005) MAP kinase pathways. *J.Cell Sci.* 118(Pt 16):3569-3572.
2. Chang L & Karin M (2001) Mammalian MAP kinase signalling cascades. *Nature* 410(6824):37-40.
3. Chen Z, *et al.* (2001) MAP kinases. *Chem.Rev.* 101(8):2449-2476.
4. Nishida E & Gotoh Y (1993) The MAP kinase cascade is essential for diverse signal transduction pathways. *Trends Biochem.Sci.* 18(4):128-131.
5. Songyang Z, *et al.* (1996) A structural basis for substrate specificities of protein Ser/Thr kinases: primary sequence preference of casein kinases I and II, NIMA, phosphorylase kinase, calmodulin-dependent kinase II, CDK5, and Erk1. *Mol.Cell Biol.* 16(11):6486-6493.
6. Ferrell JE, Jr. & Machleder EM (1998) The biochemical basis of an all-or-none cell fate switch in Xenopus oocytes. *Science* 280(5365):895-898.
7. Xiong W & Ferrell JE, Jr. (2003) A positive-feedback-based bistable 'memory module' that governs a cell fate decision. *Nature* 426(6965):460-465.
8. Santos SD, Verveer PJ, & Bastiaens PI (2007) Growth factor-induced MAPK network topology shapes Erk response determining PC-12 cell fate. *Nat.Cell Biol.* 9(3):324-330.
9. Daniels MA, *et al.* (2006) Thymic selection threshold defined by compartmentalization of Ras/MAPK signalling. *Nature* 444(7120):724-729.
10. Lin J, Harding A, Giurisato E, & Shaw AS (2009) KSR1 modulates the sensitivity of mitogen-activated protein kinase pathway activation in T cells without altering fundamental system outputs. *Mol.Cell Biol.* 29(8):2082-2091.
11. Ferrell JE, Jr. & Bhatt RR (1997) Mechanistic studies of the dual phosphorylation of

mitogen-activated protein kinase. *J.Biol.Chem.* 272(30):19008-19016.

12. Huang CY & Ferrell JE, Jr. (1996) Ultrasensitivity in the mitogen-activated protein kinase cascade. *Proc.Natl.Acad.Sci.U.S.A* 93(19):10078-10083.

13. Markevich NI, Hoek JB, & Kholodenko BN (2004) Signaling switches and bistability arising from multisite phosphorylation in protein kinase cascades. *J.Cell Biol.* 164(3):353-359.

14. Haystead TA, Dent P, Wu J, Haystead CM, & Sturgill TW (1992) Ordered phosphorylation of p42mapk by MAP kinase kinase. *FEBS Lett.* 306(1):17-22.

15. Burack WR & Sturgill TW (1997) The activating dual phosphorylation of MAPK by MEK is nonprocessive. *Biochemistry (Mosc.)* 36(20):5929-5933.

16. Colman-Lerner A, *et al.* (2005) Regulated cell-to-cell variation in a cell-fate decision system. *Nature* 437(7059):699-706.

17. Poritz MA, Malmstrom S, Kim MK, Rossmeissl PJ, & Kamb A (2001) Graded mode of transcriptional induction in yeast pheromone signalling revealed by single-cell analysis. *Yeast* 18(14):1331-1338.

18. Takahashi S & Pryciak PM (2008) Membrane localization of scaffold proteins promotes graded signaling in the yeast MAP kinase cascade. *Curr.Biol.* 18(16):1184-1191.

19. Mackeigan JP, Murphy LO, Dimitri CA, & Blenis J (2005) Graded mitogen-activated protein kinase activity precedes switch-like c-Fos induction in mammalian cells. *Mol.Cell Biol.* 25(11):4676-4682.

20. Whitehurst A, Cobb MH, & White MA (2004) Stimulus-coupled spatial restriction of extracellular signal-regulated kinase 1/2 activity contributes to the specificity of signal-response pathways. *Mol.Cell Biol.* 24(23):10145-10150.

21. Levchenko A, Bruck J, & Sternberg PW (2000) Scaffold proteins may biphasically affect the levels of mitogen-activated protein kinase signaling and reduce its threshold properties. *Proc.Natl.Acad.Sci.U.S.A* 97(11):5818-5823.

22. Burack WR & Shaw AS (2000) Signal transduction: hanging on a scaffold. *Curr.Opin.Cell Biol.* 12(2):211-216.

23. Kolch W (2005) Coordinating ERK/MAPK signalling through scaffolds and inhibitors. *Nat.Rev.Mol.Cell Biol.* 6(11):827-837.

24. Patwardhan P & Miller WT (2007) Processive phosphorylation: mechanism and biological importance. *Cell Signal.* 19(11):2218-2226.

25. Shaw AS & Filbert EL (2009) Scaffold proteins and immune-cell signalling. *Nat.Rev.Immunol.* 9(1):47-56.

26. Amit I, *et al.* (2007) A module of negative feedback regulators defines growth factor signaling. *Nat.Genet.* 39(4):503-512.

27. Kinoshita E, Kinoshita-Kikuta E, Takiyama K, & Koike T (2006) Phosphate-binding tag, a new tool to visualize phosphorylated proteins. *Mol.Cell Proteomics.* 5(4):749-757.

28. Schilling M, *et al.* (2009) Theoretical and experimental analysis links isoform-specific ERK signalling to cell fate decisions. *Mol.Syst.Biol.* 5:334.

29. Ellis RJ (2001) Macromolecular crowding: an important but neglected aspect of the intracellular environment. *Curr.Opin.Struct.Biol.* 11(1):114-119.

30. Minton AP (2006) How can biochemical reactions within cells differ from those in test tubes? *J Cell Sci.* 119(Pt 14):2863-2869.

31. Shtilerman MD, Ding TT, & Lansbury PT, Jr. (2002) Molecular crowding accelerates fibrillization of alpha-synuclein: could an increase in the cytoplasmic protein

concentration induce Parkinson's disease? *Biochemistry (Mosc.)* 41(12):3855-3860.

32. Takahashi K, Tanase-Nicola S, & ten Wolde PR (2010) Spatio-temporal correlations can drastically change the response of a MAPK pathway. *Proc.Natl.Acad.Sci.U.S.A* 107(6):2473-2478.

33. Reynolds AR, Tischer C, Verveer PJ, Rocks O, & Bastiaens PI (2003) EGFR activation coupled to inhibition of tyrosine phosphatases causes lateral signal propagation. *Nat.Cell Biol.* 5(5):447-453.

34. Fujioka A, *et al.* (2006) Dynamics of the Ras/ERK MAPK cascade as monitored by fluorescent probes. *J.Biol.Chem.* 281(13):8917-8926.

Fig. legends

Fig. 1. ERK phosphorylation *in vitro*. (A) Schematic representation of the input-output response of ERK MAP kinase. The distributive phosphorylation model leads to switch-like response. On the other hand, no model is currently validated for the graded response of ERK, which is observed in mammalian cells and yeast. (B) His-tagged MEK1-SDSE and GST-ERK2-KR were incubated with ATP for the indicated periods, followed by Phos-tag western blotting analysis. All phospho-isoforms of ERK were detected by anti-GST rabbit antibody (upper) and IRDye680-conjugated anti-rabbit IgG antibody as a secondary antibody. The positions of the phospho-isoforms of ERK are indicated at right (SI Appendix, Fig. S4). pTpY-ERK was simultaneously detected by anti-pTpY-ERK mouse antibody (middle) and IRDye800-conjugated anti-mouse IgG antibody as a secondary antibody. The lower image is the merged image (Red: ERK, Green: pTpY-ERK). (C) The phospho-isoforms of ERK were quantified and plotted with SD (n = 3).

Fig. 2. Numerical and experimental analyses of the distributive phosphorylation model. (A) Schematic representation of the distributive model (see SI Appendix, Fig. S8A in detail). (B and C) Results of numerical simulations are represented based on experimentally determined parameters (SI Appendix, Tables S1 and S2). (B) Concentrations of np-ERK (blue), pY-ERK (green), pTpY-ERK (red) and pT-ERK (orange) are plotted against time. The kcat/Km value of cRaf kinase for MEK phosphorylation (Raf_kphos) is 1.0×10^6 [/M/sec]. (C) Concentrations of the phospho-isoforms of ERK are plotted against the Raf_kphos value at time = 10 [minutes]. (D

and E) After serum starvation, HeLa cells were stimulated with 1.0 x 10^{-5} g/l EGF at the indicated time period. (D) Cell lysates were separated by SDS-polyacrylamide gel containing Phos-tag and probed with an anti-ERK antibody. (E) The amounts of np-ERK2 (blue), pY-ERK2 (green), and pTpY-ERK2 (red) are plotted against time after EGF stimulation with SD (n = 3). (F and G) After serum starvation, HeLa cells were stimulated with the indicated concentration of EGF for 7.5 min. (F) Cell lysates were analyzed by Phos-tag western blot analysis as in D. (G) The amounts of np-ERK2 (blue), pY-ERK2 (green), and pTpY-ERK2 (red) are plotted as a function of the EGF concentration with SD (n = 5).

Fig. 3. Computational simulation of the processive phosphorylation model. (A) Schematic representation of the processive model (see SI Appendix, Fig. S8B in detail). (B) Results of numerical simulations are represented based on experimentally determined parameters (SI Appendix, Tables S1 and S2). Time series of np-ERK (blue), pY-ERK (green), pTpY-ERK (red) and pT-ERK (orange) concentrations are plotted at Raf_kphos value = 1.0 x 10^{6} [/M/sec]. (C) Concentrations of the phospho-isoforms of ERK are plotted as a function of Raf_kphos value at time = 10 (min).

Fig. 4. Validation of the processive model by pY-ERK dynamics. (A and B) Numerical simulations were performed based on the distributive model (A) and the processive model (B) in the absence (left column) or presence of the inhibition of all phosphatase reactions (right column). Time series of np-ERK (blue), pY-ERK (green), pTpY-ERK (red) and pT-ERK (orange) concentrations are plotted at Raf_kphos value = 1.0 x 10^{6} [/M/sec]. Maximal levels of pY-ERK without inhibition are indicated by gray dashed lines. (C and D) After serum starvation, HeLa

cells were treated with mock or 1.0 x 10^{-7} M Calyculin A and 1.0 x 10^{-4} M bpV for 2 min, followed by 1.0 x 10^{-5} g/l EGF for the indicated time period. (C) Cell lysates were separated by electrophoresis in SDS-polyacrylamide gels containing Phos-tag and probed with an anti-ERK antibody. (D) Time series of np-ERK2 (blue), pY-ERK2 (green), and pTpY-ERK2 (red) concentrations without (left) or with (right) phosphatase inhibitors are plotted after EGF stimulation with SD (n = 4).

Fig. 5. Validation of the processive model by input-output response. (A and B) Serum-starved HeLa cells were stimulated with the different concentration of EGF (blue, 0.01; cyan, 0.03; green, 0.1; yellow, 0.3; orange, 1.0; pink, 3.0; red, 10 (x 10^{-6} [g/l])) or 2.0 x 10^{-5} M U0126 (black) for 5 min, and then stained with anti-pTpY-ERK1/2 antibody. (A) Fluorescent signals in each cell are represented in a histogram, demonstrating unimodal distributions (n > 90 cells). (B) The average fluorescent intensities are plotted as a function of EGF concentration with SD. Hill coefficient value, nH, was obtained by curve fitting with standard Hill equation (black line). (C) The average of fraction of pTpY-ERK are plotted as a function of EGF concentration with SD (n = 5). This data is same as shown in Fig. 2G (red line). (D) The average of fraction of pTpY-ERK was plotted as a function of ratio value of phosphorylated MEK1/2 to total MEK1/2 with SD (n = 5). (E and F) The pTpY-ERK concentration at time = 10 (min) after stimulation in distributive (E) and processive (F) model are plotted as a function of phosphorylated MEK concentration.

Fig. 6. Effect of molecular crowding on processive phosphorylation. (A and B) ERK was phosphorylated by MEK in the absence (A) or presence (B) of 15% (w/v) polyethylene glycol (PEG) in vitro and were subjected to Phos-tag western blotting analysis. (C and D) The

concentrations of phospho-isoforms of ERK in A and B are plotted as dots against time. Concentration of constitutively active mutant of MEK (1.0×10^{-7} M) used in these experiments is indicated by gray dashed lines. The same experiments were repeated four times with reproducible results, and representative results are shown. Lines represent the concentration of phospho-isoforms of ERK obtained by fitting the processive model in panel E with the experimental data. The fitted parameters of processivity (p) and crowding factor (c) are represented. (E) Schematic representation of processive phosphorylation. p and c indicate processivity ($0<p<1$) and crowding factor, respectively. (F) Schematic view of quasi-processive model under the condition of molecular crowding.

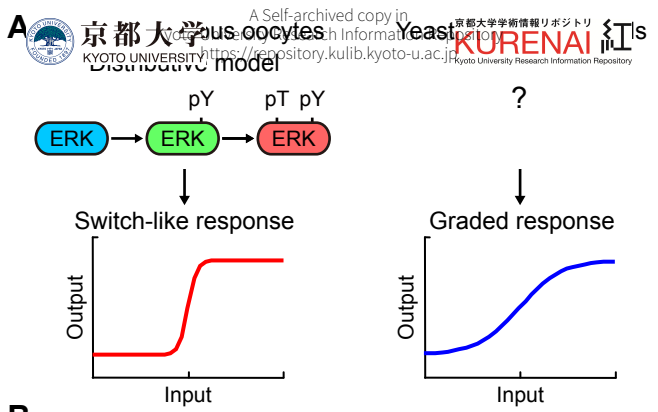

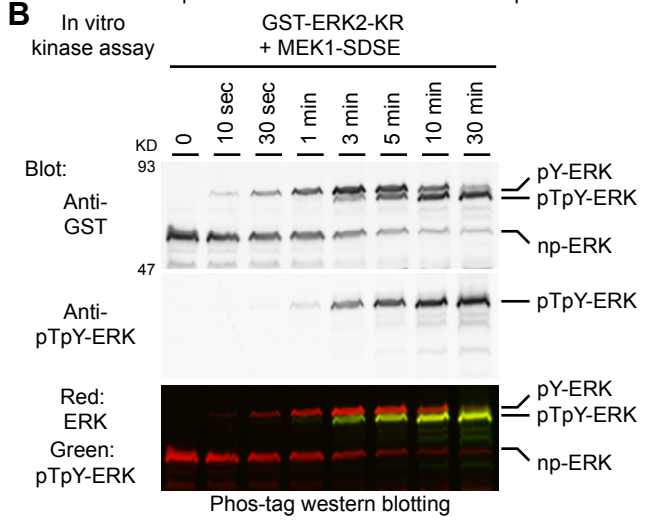

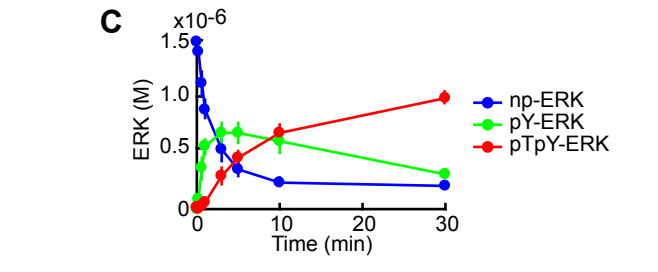

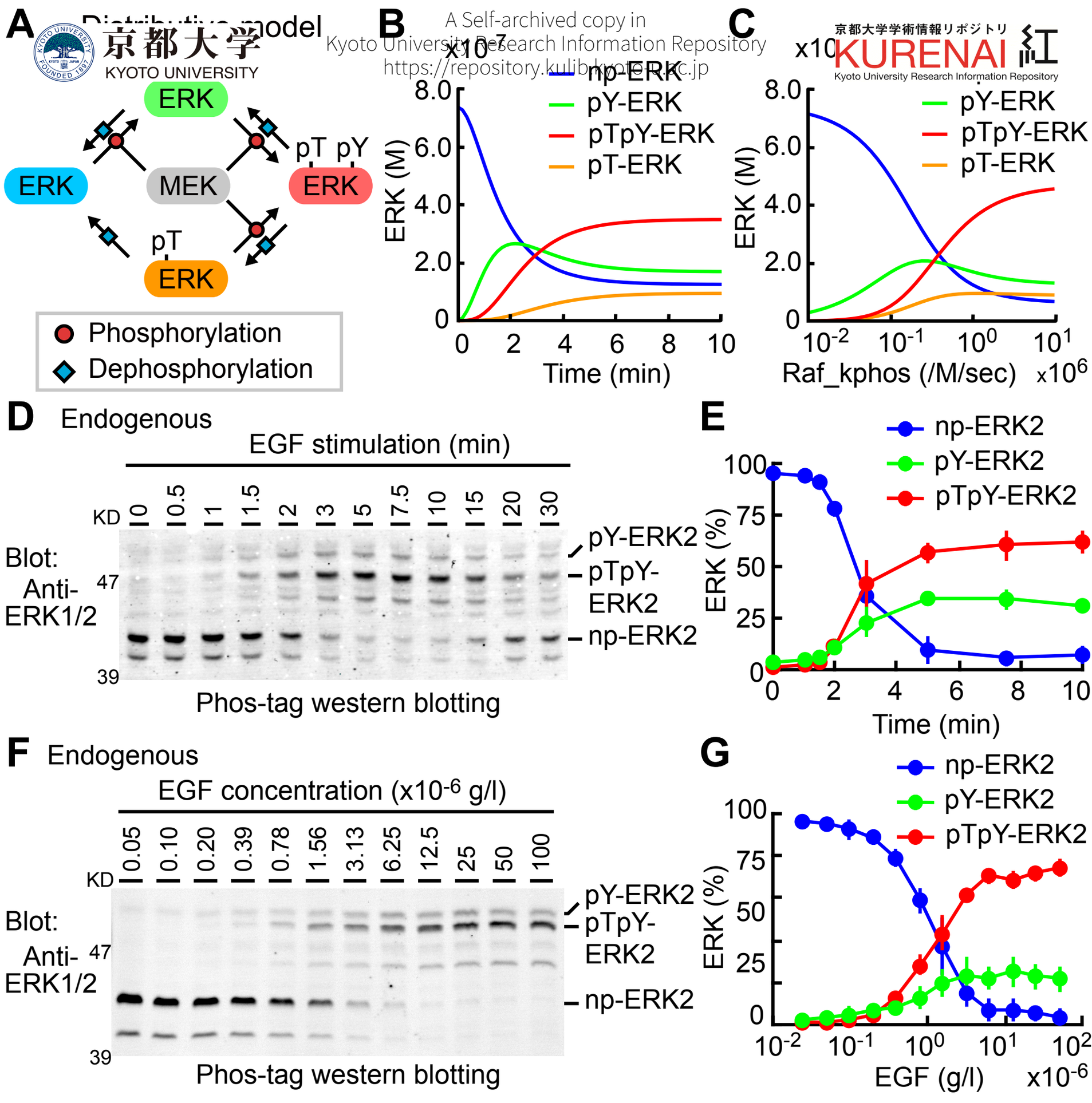

Processive model

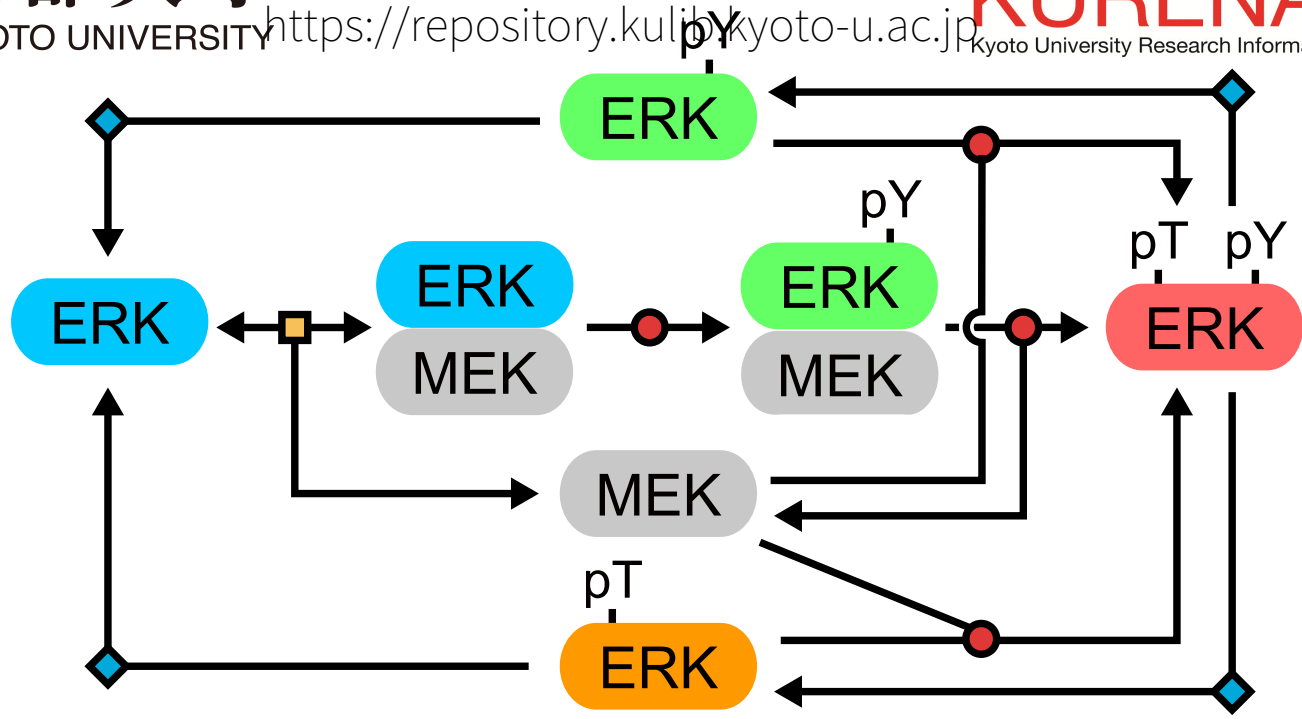

Phosphorylation
Dephosphorylation
Association/dissociation

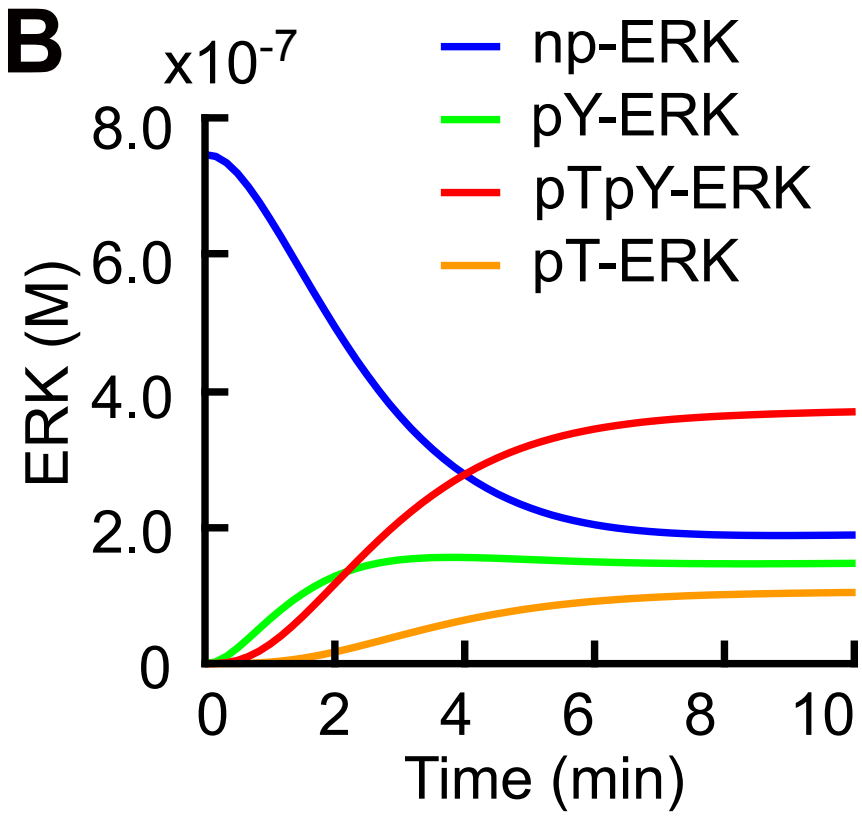

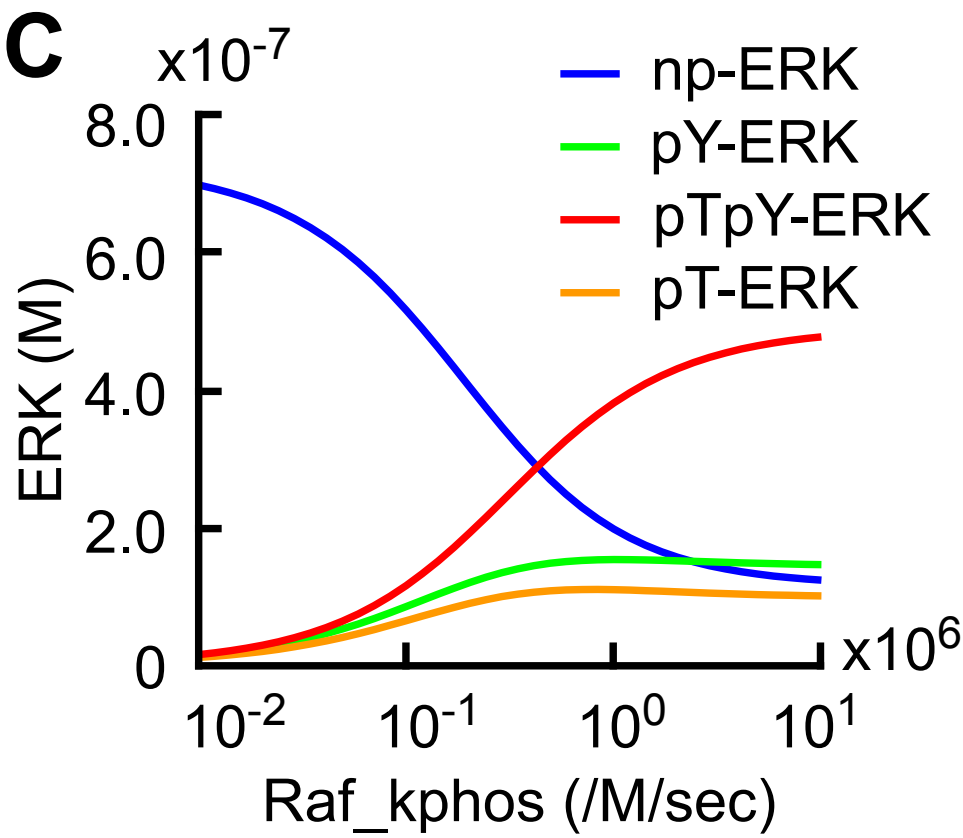

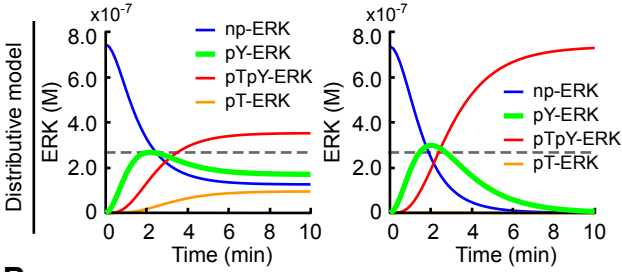

B

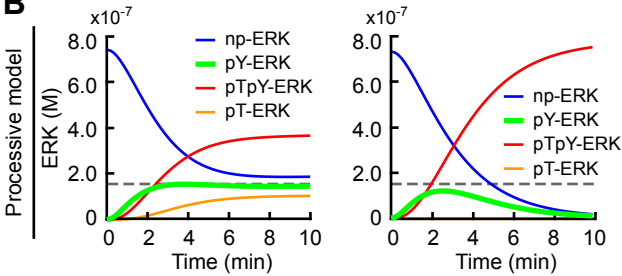

C Endogenous

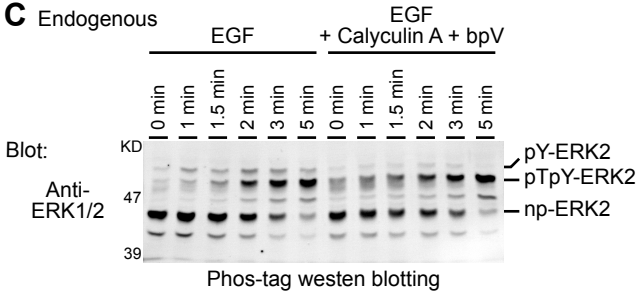

D

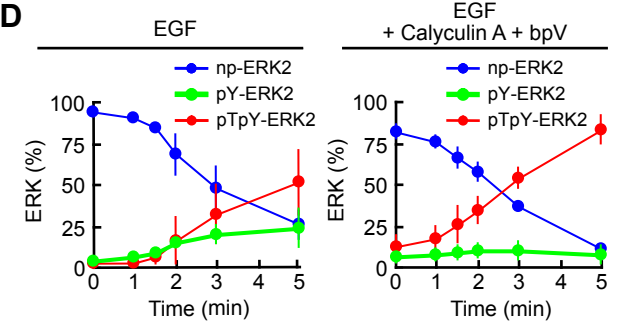

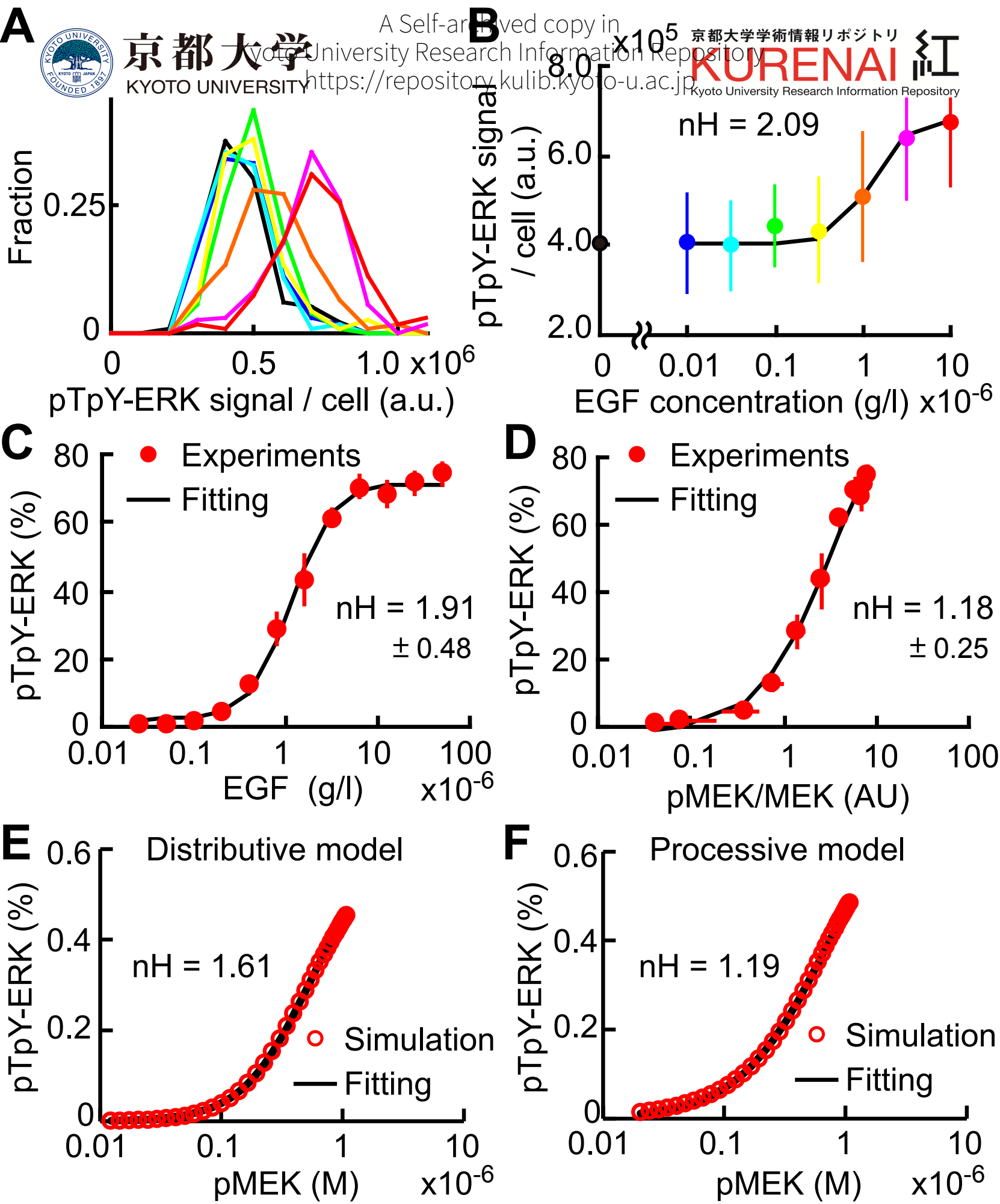

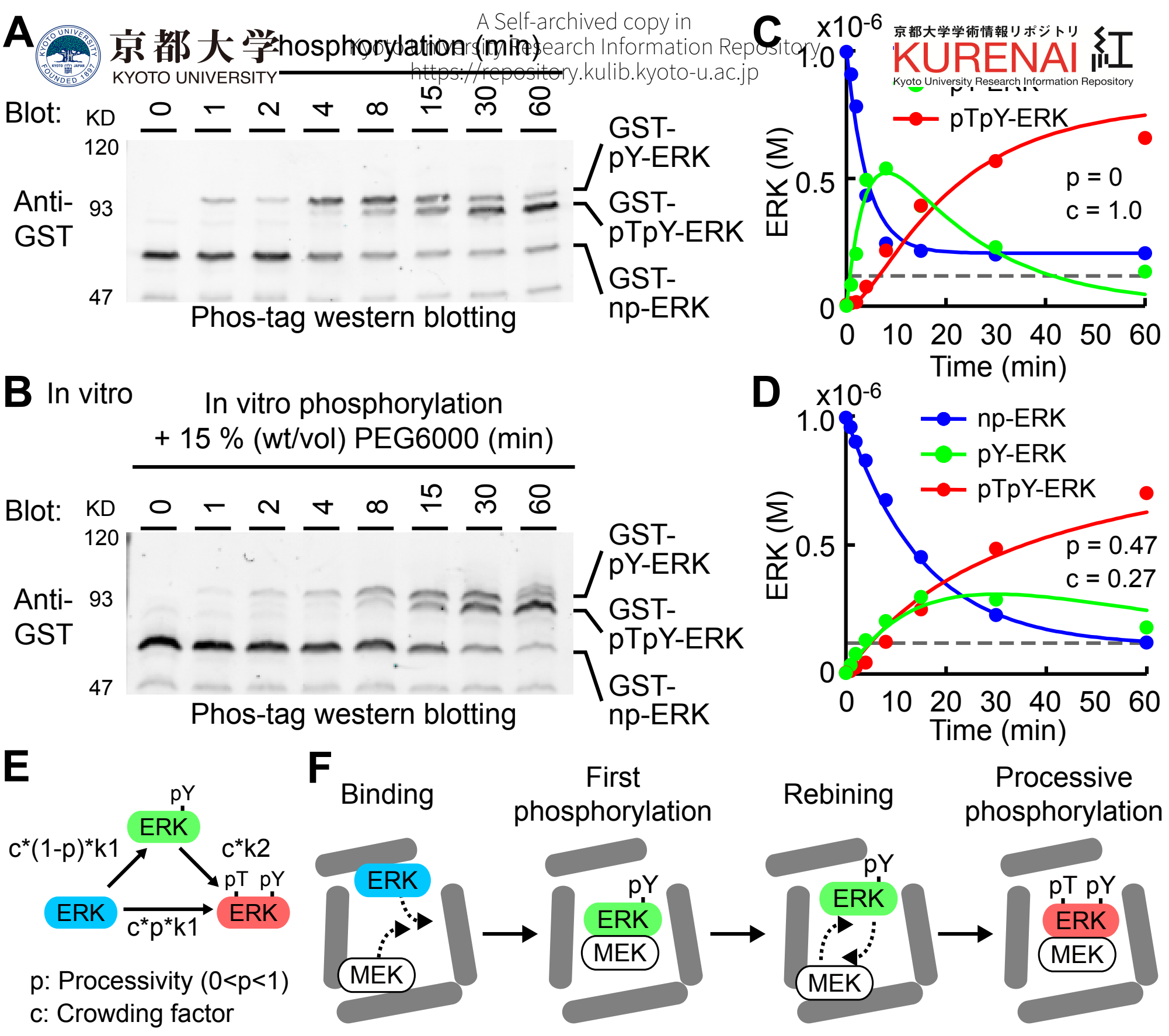

Supporting Information Appendix:

Processive phosphorylation of ERK MAP kinase in mammalian cells.

Kazuhiro Aoki, Masashi Yamada, Katsuyuki Kunida, Shuhei Yasuda, and Michiyuki Matsuda

SI Text

Dephosphorylation rates of ERK in the cytoplasm and nucleus. We determined eight dephosphorylation rates of ERK; i.e., pTpY-ERK→pY-ERK, pTpY-ERK→pT-ERK, pY-ERK→np-ERK, and pT-ERK→np-ERK in each of two compartments, i.e., the cytoplasm and nucleus (Fig. S6). Because several phosphatases, including PTP1B, PP2A, and DUSPs, have reported to be involved in ERK dephosphorylation (1), we attempted to measure the rate constant [/sec] of each dephosphorylation pathway for the cytoplasm and nucleus as the mass of phosphatases. To this end, we established HeLa cell lines stably expressing ERKs tagged with a nuclear export sequences (NES) or a nuclear localization signals (NLS). The cells were treated with EGF followed by an MEK inhibitor, PD184352, to measure the dephosphorylation rates (Fig. S6A, left column). Calyculin A, a serine/threonine phosphatase PP1/PP2A inhibitor, or bpV, a tyrosine phosphatase inhibitor, was also used to discriminate the two dephosphorylation reactions (Fig. S6A, center and right columns). Finally, the time constants for each dephosphorylation pathway were determined by curve-fitting the concentration of phospho-isoforms of ERK with a single exponential decay function (Fig. S6B-K). Notably, we observed accumulation of pT-ERK and pY-ERK in the presence of Calyculin A and bpV, respectively (Fig. S6A). This observation indicated that the dephosphorylation of pTpY-ERK was primarily mediated by serine/threonine phosphatases and tyrosine phosphatases, rather than dual-specificity phosphatases, at least in our experimental conditions. Furthermore, the dephosphorylation rate of MEK was also determined and included in our simulation model (Fig. S7). Of note, we neglected the effect of phosphatase inhibitors on Raf and MEK, because they will not affect the mode of ERK phosphorylation.

Involvement of Scaffold proteins in the processive model. Feasible candidates for the determinant of the processive phosphorylation include scaffold proteins, which regulate assembly of two or more components of signaling pathways and consequently change the mode of phosphorylation (2-6). To examine the contribution of scaffold proteins to the processive phosphorylation, we depleted KSR, MP-1, IQGAP1, Paxillin, or β-arrestin1/2 in HeLa cells by siRNA-mediated gene knockdown (7-11). The depletion of each scaffold protein could affect the phosphorylation efficiency of ERK in HeLa cells stimulated with EGF, but not alter the mode of ERK phosphorylation, namely processive phosphorylation, to the detectable level (Fig. S14). For this reason, at this moment, we failed to obtain any evidence that scaffold proteins cause processive phosphorylation in mammalian cells.

SI Materials and Methods

Plasmids. The cDNA of Xenopus MEK1 or Xenopus ERK2 was inserted into pCXN2-mVenus or pCXN2-mCFP vector to generate pCXN2-mVenus-MEK1, pCXN2-mCFP-MEK1, or pCXN2-mCFP-ERK2 (Fig. S2). Monomeric Venus (mVenus) or CFP (mCFP) was fused at the N-terminus of these vectors. The cDNA of FKBP (12) was introduced into these vectors to obtain pCXN2-mVenus-MEK1-FKBP and pCXN2-mVenus-ERK2-FKBP (Fig. S3). Threonine or tyrosine within the activation loop of ERK2 was replaced with alanine and phenylalanine, respectively, to obtain pCXN2-mVenus-ERK2T188A-FKBP and pCXN2-mVenus-ERK2Y190F-FKBP, respectively (Fig. S3). pCAGGS-FLAG-FRB-NES was designed to express FLAG tag, the FKBP-rapamycin-binding (FRB) domain of the mammalian target of rapamycin, and the nuclear export sequence (NES) of HIV rev protein (LQLPPLERLTLD) from the N-terminus. The cDNAs of human Histon H1 (the kind gift of Dr. Ishikawa) and FRB were prepared by PCR and subcloned into pERedNLS vector (pERedNLS-H1-FRB) (13) (Fig. S3). The cDNA of mouse ERK2 or human MEK1 was subcloned into the modified pCX4bsr or pCX4puro vector (14) to generate pCX4bsr-NES-FLAG-ERK2-mVenus, pCX4bsr-FLAG-ERK2-mCFP-NLS, and pCX4puro-NLS-FLAG-MEK1.
pCX4bsr-NES-FLAG-ERK2-mVenus encoded NES, FLAG tag, ERK2, and mVenus from the N-terminus (Fig. S6). pCX4bsr-FLAG-ERK2-mCFP-NLS was designed to express FLAG tag, ERK2, mCFP and the nuclear localization signal (NLS) of SV40 large T antigen (GGPPKKKPKVEDP). pCX4puro-NLS-FLAG-MEK1 encoded NLS, FALG tag and MEK1 from the N-terminus. A fragment of the kinase-deficient mutant of Xenopus ERK2 (ERK2-KR) was inserted into the pGEX4T3 vector to obtain pGEX4T3-ERK2-KR (Figs. 1, 6, S2, and S5). The cDNA of the wild type Xenopus MEK1 (MEK1WT), constitutively active mutant MEK1 (MEK1SDSE), or human PTP1B (the kind gift of Dr. B. Neel) was subcloned into the pET-12HisFLAG vector, which was designed to express double histidine hexamer-tagged FLAG peptide at the N-terminus (Figs, 1, 6, S2, S4, S5, and S12).

Cells, reagents and antibodies. HeLa cells were purchased from the Human Science Research Resources Bank (Sennan-shi, Japan). HeLa cells were maintained in DMEM (Sigma-Aldrich, St. Louis, MO) supplemented with 10% fetal bovine serum (FBS). HEK-293F cells were purchased from Invitrogen (San Diego, CA), and maintained in FreeStyle 293 Expression Medium (Invitrogen). Expression plasmids were transfected into HeLa cells by 293Fectin (Invitrogen) according to the manufacturer's instructions. EGF was purchased from Sigma-Aldrich. Calyculin A, bpV(phen), ZM336372, and

anisomycin were purchased from Calbiochem (La Jolla, CA). PD184352 was obtained from Toronto Research Chemicals (Ontario, Canada). Phos-tag acrylamide was obtained from the Phos-tag Consortium (http://www.phos-tag.com/). Fluorescent beads for calibration of Venus and CFP were purchased from Invitrogen (InSpeck Green (505/515) Microscope Image Intensity Calibration Kit) and from Polyscience (Fluoresbrite Plain YG 0.1 micron Microspheres) (Warrington, PA). Anti-MEK1/2, anti-ERK1/2, anti-p38, anti-phospho-MEK1/2 (Ser217/221), anti-phospho-ERK1/2 (Thr202/Tyr204 and Thr185/Tyr187, respectively), and anti-phsopho-p38 (Thr180/Tyr182) were purchased from Cell Signaling Technology (Beverly, MA). Anti-cRaf monoclonal antibodies came from BD Transduction Laboratories (San Jose, CA). Anti-pY-ERK and anti-pT-ERK monoclonal antibodies were purchased from Sigma. Anti-GFP and anti-GST rabbit sera were prepared in our laboratory (15, 16). LI-COR blocking buffer, IRDye680- and IRDye800-conjugated anti-rabbit and anti-mouse IgG secondary antibodies were obtained from LI-COR Bioscience (Lincoln, NE). Polyethylene glycol 6000 was purchased from Hampton Research (Aliso Viejo, CA).

Establishment of stable cell lines. For generation of HeLa cell lines stably expressing ectopic proteins, we utilized a retroviral system. The murine ecotropic retrovirus receptor (EcoVR) was first introduced into HeLa cells by retroviruses produced from BOSC23 cells, which had been transfected with pCX4hyg-EcoVR, the packaging plasmid pGP, and the envelope plasmid pVSV-G (14). The HeLa cells stably expressing EcoVR were selected by Hygromycin. Then, HeLa-EcoVR cells were infected with retroviruses obtained from pCX4bsr-NES-FLAG-ERK2-mVenus-, pCX4bsr-FLAG-ERK2-mCFP-NLS-, or CX4puro-NLS-FLAG-MEK1-transfected BOSC23 cells (Fig. S6).

Purification of recombinant proteins and in vitro kinase assay. Recombinant proteins fused to GST-tag and His-tag were expressed in E. coli strain BL21-DE3 from pGEX- and pET-derived vectors and purified as described previously (16). GST-tagged human MEK1, GST-tagged human ERK2, and GST-tagged human cRaf deleted with the N-terminus (kinase active mutant) were purchased from Millipore (Bedford, MA). For preparation of GST-pT-ERK2, plasmids of both pGEX-ERK2-KR and pET-12HisFLAG-MEK1SDSE were cotransformed into E-coli strain BL21-DE3. Fully phosphorylated-GST-ERK2 (pTpY-ERK2) was purified and incubated with recombinant 12HisFLAG-PTP1B to dephosphorylate phospho-tyrosine in dephosphorylation buffer (100 mM Tris [pH 7.5], 100 mM NaCl, 1 mM EDTA, 2 mM DTT). The GST-pT-ERK2 was then further purified. For in vitro kinase assay, GST-ERK2 or GST-pT-ERK2 with 12HisFLAG-MEK1SDSE was incubated in in vitro kinase buffer (50 mM Tris [pH 7.5], 10 mM MgCl2, 0.02% BSA 0.2 mM DTT). The reaction was started by adding 5 x ATP solution (5 mM ATP, 50 mM MgCl2, 25 mM Tris [pH 7.2], 0.15 M NaCl) and stopped at the indicated time point by adding SDS sample buffer.

Preparation of cytoplasmic extract. For preparation of cytoplasmic extract, HEK-293F cells were collected by centrifugation. The packed cells were snap-frozen, followed by rapid thawing in water bath. After centrifugation, the supernatant was collected and used as cytoplasmic extract. The extract was diluted 10-fold for in vitro kinase reaction.

Immunostaining. Cells were fixed with 3.7% formaldehyde and permeabilized with 0.2% Triton X-100. After having been soaked for 1 h in phosphate-buffered saline (PBS) containing 3% BSA and 0.02% Triton X-100, the samples were incubated for 1 h at room temperature with 5 μg/ml anti-pTpY-ERK antibodies, washed with PBS, and then incubated for 30 min at room temperature with Alexa 488 anti-mouse IgG,. The samples were washed with PBS containing 0.2% Tween 20, and imaged with an Olympus FV1000 microscope.

Measurement of the dissociation constant by intermolecular FRET assay. First, images of YFP, CFP and FRET were acquired, and then corrected FRET (cFRET) images were created by subtracting the contributions of cross-excitation and bleed-through as follows:

$$[cFRET] = [FRET] - (0.089 \cdot [YFP]) - (0.55 \cdot [CFP]),$$

where 0.089 and 0.55 indicate the degree of cross-excitation and spectral bleed-through under our microscopic conditions, respectively (17). cFRET and the cFRET/YFP ratio indicate the amount of bound protein and the fraction of acceptor protein that contribute to FRET, respectively. Concentrations of fluorescent proteins were evaluated by calibrated fluorescent beads as described previously (18). The fraction of ERK-bound MEK (Bound MEK/Total MEK) in individual cells was calculated as follows:

$$\frac{Bound\_MEK}{Total\_MEK} = \frac{1}{0.16} \cdot \frac{1}{0.57} \cdot \frac{[cFRET]}{[YFP]},$$

where 0.16 is the maximal FRET efficiency between mVenus-MEK1 and mCFP-ERK2, and 0.57 is a quantum yield of Venus (19). The dissociation constant value was calculated by curve fitting the plotted data with the following equation:

$$\frac{Bound\_MEK}{Total\_MEK} = \frac{[Free\_ERK]}{K_d + [Free\_ERK]},$$

where K_d is a dissociation constant.

In vitro binding assay. Various concentration of GST-ERK2KR and 100 nM 12His-FLAG-MEK1WT were incubated with in vitro binding buffer (PBS, 0.1% Tween-20, 1 mM MgCl2, 40 mM imidazole). Bound protein was pulled down by Ni-NTA agarose beads (Qiagen, Valencia, CA), washed with in vitro binding buffer three times, and eluted with 200 mM imidazole-containing PBS. Each eluate was analyzed by SDS-PAGE and western blotting.

Surface plasmon resonance assay. Surface plasmon resonance spectroscopy was performed with a BIAcore-X optical biosensor instrument (Biacore AB, Uppsala, Sweden)

using a NTA sensor chip (NTA bound to a solid support) as described previously (20). Briefly, surface plasmon resonance buffers were as follows: (i) regeneration buffer: 10 mM Hepes, 0.15 M NaCl, 0.35 M EDTA, pH 7.4; (ii) nickel buffer: 500 μM NiSO4 in running buffer; (iii) running buffer: PBS with 1 mM MgCl2, 0.1 % (v/v) Surfactant 20, pH 7.4. Ligand (12His-tagged MEK1WT) and analyte (GST-tagged ERK2KR) were dissolved in running buffer. All reactions were done at 25 °C. The data were analyzed using BIAevaluation 3.0 software (Biacore AB) and kinetic analyses of primary sensorgrams were carried out by global fitting using a modified-heterogeneous binding model to consider non-specific binding of the analyte to Ni-NTA chip sensor.

Nucleocytoplasmic shuttling rates of MEK and ERK. To measure nuclear import and export rates, we used a rapamycin-induced dimerization system of an FK506-binding protein (FKBP12 or FKBP) and FRB domain. For measurement of nuclear import rates, Histon H1-fused FRB (H1-FRB) was employed as a binder for FKBP-fused proteins. Similarly, the nuclear export rate of ERK was determined with an FRB fused to the nuclear export sequence (NES). We measured nuclear import and export rates of phospho-isoforms of ERK as follows: phosphorylation of ERK2T188A or ERK2Y190F was induced by the stimulation of EGF and bpV for 10 min. Then, Rapamycin was added to the cells in order to trap phosphorylated ERK in nucleus or cytoplasm. The fraction of phospho-isoforms of ERK was measured by Phos-tag Western blotting analysis (Fig. S3A). We utilized this fraction value for the exponential curve fitting. Furthermore, the contribution of MEK-dependent active nuclear export of ERK was ignored, because the nuclear import rate of MEK (4.0×10^{-4} [/sec]) was considerably slower than the nuclear import and export rates of ERK under the time scale used in our simulation model (~30 min). From these data, we show that pTpY-ERK seems to be actively imported into the nucleus. Unexpectedly, the nuclear export rate of pT-ERK is larger than those of the other phospho-isoforms. Thus, both the fast import of pTpY-ERK and the fast export of pT-ERK contribute to the increase in pTpY-ERK accumulation in HeLa cells.

Phosphorylation rates of ERK in vitro. Each experiment included a series of diluted GST-ERK concentration as shown in Fig. S5. These eluates were subjected into Phos-tag western blotting. The amounts of phospho-isoforms of ERK were quantified and fitted by global least-square regression algorithm to solutions of following differential equations with Microsoft Excel Solver:

$$d[np-ERK]/dt = -kf_1 \cdot [MEK] \cdot [np-ERK]$$
$$d[pY-ERK]/dt = kf_1 \cdot [MEK] \cdot [np-ERK] - kf_2 \cdot [MEK] \cdot [pY-ERK]$$
$$d[pTpY-ERK]/dt = kf_2 \cdot [MEK] \cdot [pY-ERK]$$

where [MEK], [np-ERK], [pY-ERK], and [pTpYhK] are concentration of MEK, np-ERK, pY-ERK, and pTpY-ERK, respectively. kf1 and kf2 are phosphorylation rate constants [/M/sec], which are enzymatically identical to kcat/Km at substrate concentrations significantly lower than Km. Initial velocity of the phosphorylation was plotted against the substrate concentration (Fig. S5C). The initial velocity was not saturated up to 1.5×10^{-6} M, indicating that the Michaelis constant of the first phosphorylation step is over this range. Therefore, we assumed the linear reaction rates of ERK phosphorylation at least in the range of ERK concentrations.

siRNA for scaffold proteins and quantitative RT-PCR. Scramble siRNA and validated siRNAs for human KSR1 (#1 and #2) were purchased from Invitrogen (San Diego, CA). siRNAs for human MP1, IQGAP1, Paxillin, β-arrestin1, and β-arrestin2 were obtained Santa Cruz Biotechnology (Santa Cruz, CA). HeLa cells were transfected with 20 μM control siRNA or siRNA for a scaffold protein by Lipofectamine RNAiMAX (Invitrogen). Three days after transfection, total RNA was purified by RNeasy Mini Kit (QIAGEN, Hilden, Germany), and reverse-transcribed by High Capacity cDNA Reverse Transcription kit (Applied Biosystems, Foster City, CA) according to the manufacture's protocol. Then, expression levels of scaffold protein and GAPDH were analyzed by SYBR GreenER qPCR SuperMix (Invitrogen) with ABI PRISM7000 Sequence Detection System (Applied Biosystems). Primers used for real time PCR analysis were listed as follows. GAPDH: (Fw) 5'-GAGTCCACTGGCGTCTTCAC-3' and (Rv) 5'-GTTCACACCCATGACGAACA-3', KSR1: (Fw) 5'-TCTCCCACCCTGGACACTT-3' and (Rv) 5'-GAGGAAGAAAGCCCCTGGT-3' MP1: (Fw) 5'-TGTCAGATAGAGATGGAGTACCTGTT-3' and (Rv) 5'-AAACCAGGTCGCAAAGCAT-3', IQGAP1: (Fw) 5'-TGTGCAAAATTCTATGCAGCTT-3' and (Rv) 5'-GGCAGTCACCCCAGAGATAG-3', Paxillin: (Fw) 5'-CAGCAGACACGCATCTCG-3' and (Rv) 5'-GAGCTGCTCCCTGTCTTCC-3', β -arrestin1: (Fw) 5'-ACTATGAAGTCAAAGCCTTCTGC-3' and (Rv) 5'-GGATGACCAGACGCACAGA-3', β -arrestin2: (Fw) 5'-GGAAACTCAAGCACGAGGAC-3' and (Rv) 5'-CTTGTTGGCACCCTCCTTC-3'

Kinetic modeling and numerical simulation. All kinetic reactions were described with mass action kinetics by using CellDesigner (version 4.0 beta) (21) (Fig. 3A, 4A, and S8). Then, the ordinary differential equations and parameters were exported to the MATLAB software (version R2008b or R2010b; The Mathworks Inc., Natick, MA) through Systems Biology Workbench (version 2.7.8) (22). Numerical simulation was performed by MATLAB software with ode23 function. To ensure consistency of simulation results with western blot results, concentration of phospho-isoforms of ERK was represented by summing all ERK species in nucleus and cytoplasm.

3Parameter search and evaluation. Parameter search was performed by using fminseach function in MATLAB (Fig. S11). The target function for parameter search was residual sum of square (RSS) between the experimental data (Fig. 2E and Fig. 4D) and simulation data in distributive model or processive model. The fminsearch function found a parameter set that minimized the RSS value to fit simulation data with experimental data. After finding optimized parameters in each of the distributive and processive models, the RSS value and the

number of parameters for optimization were utilized to calculate Akaike information criterion (AIC) value for ranking which of models was reasonable (23).

SI References

1. Zhou B, Wang ZX, Zhao Y, Brautigan DL, & Zhang ZY (2002) The specificity of extracellular signal-regulated kinase 2 dephosphorylation by protein phosphatases. *J.Biol.Chem.* 277(35):31818-31825.
2. Burack WR & Shaw AS (2000) Signal transduction: hanging on a scaffold. *Curr.Opin.Cell Biol.* 12(2):211-216.
3. Kolch W (2005) Coordinating ERK/MAPK signalling through scaffolds and inhibitors. *Nat.Rev.Mol.Cell Biol.* 6(11):827-837.
4. Levchenko A, Bruck J, & Sternberg PW (2000) Scaffold proteins may biphasically affect the levels of mitogen-activated protein kinase signaling and reduce its threshold properties. *Proc.Natl.Acad.Sci.U.S.A* 97(11):5818-5823.
5. Patwardhan P & Miller WT (2007) Processive phosphorylation: mechanism and biological importance. *Cell Signal.* 19(11):2218-2226.
6. Shaw AS & Filbert EL (2009) Scaffold proteins and immune-cell signalling. *Nat.Rev.Immunol.* 9(1):47-56.
7. Stewart S, *et al.* (1999) Kinase suppressor of Ras forms a multiprotein signaling complex and modulates MEK localization. (Translated from eng) *Mol. Cell. Biol.* 19(8):5523-5534 (in eng).
8. Schaeffer HJ, *et al.* (1998) MP1: a MEK binding partner that enhances enzymatic activation of the MAP kinase cascade. *Science* 281(5383):1668-1671.
9. Roy M, Li Z, & Sacks DB (2005) IQGAP1 is a scaffold for mitogen-activated protein kinase signaling. *Mol.Cell Biol.* 25(18):7940-7952.
10. Ishibe S, Joly D, Zhu X, & Cantley LG (2003) Phosphorylation-dependent paxillin-ERK association mediates hepatocyte growth factor-stimulated epithelial morphogenesis. *Mol.Cell* 12(5):1275-1285.
11. DeFea KA, *et al.* (2000) beta-arrestin-dependent endocytosis of proteinase-activated receptor 2 is required for intracellular targeting of activated ERK1/2. *J Cell Biol.* 148(6):1267-1281.
12. Aoki K, Nakamura T, Inoue T, Meyer T, & Matsuda M (2007) An essential role for the SHIP2-dependent negative feedback loop in neuritogenesis of nerve growth factor-stimulated PC12 cells. *J.Cell Biol.* 177(5):817-827.
13. Aoki K, Nakamura T, Fujikawa K, & Matsuda M (2005) Local phosphatidylinositol 3,4,5-trisphosphate accumulation recruits Vav2 and Vav3 to activate Rac1/Cdc42 and initiate neurite outgrowth in nerve growth factor-stimulated PC12 cells. *Mol.Biol.Cell* 16(5):2207-2217.
14. Akagi T, Sasai K, & Hanafusa H (2003) Refractory nature of normal human diploid fibroblasts with respect to oncogene-mediated transformation. *Proc.Natl.Acad.Sci.U.S.A* 100(23):13567-13572.
15. Ohba Y, Kurokawa K, & Matsuda M (2003) Mechanism of the spatio-temporal regulation of Ras and Rap1. *EMBO J.* 22(4):859-869.
16. Ohba Y, *et al.* (2000) Regulatory proteins of R-Ras, TC21/R-Ras2, and M-Ras/R-Ras3. *J.Biol.Chem.* 275(26):20020-20026.
17. Fujioka A, *et al.* (2006) Dynamics of the Ras/ERK MAPK cascade as monitored by fluorescent probes. *J.Biol.Chem.* 281(13):8917-8926.
18. Sugiyama Y, Kawabata I, Sobue K, & Okabe S (2005) Determination of absolute protein numbers in single synapses by a GFP-based calibration technique. *Nat.Methods* 2(9):677-684.
19. Nagai T, *et al.* (2002) A variant of yellow fluorescent protein with fast and efficient maturation for cell-biological applications. *Nat.Biotechnol.* 20(1):87-90.
20. Baekgaard L, Luoni L, De Michelis MI, & Palmgren MG (2006) The plant plasma membrane Ca2+ pump ACA8 contains overlapping as well as physically separated autoinhibitory and calmodulin-binding domains. *J.Biol.Chem.* 281(2):1058-1065.
21. Kitano H, Funahashi A, Matsuoka Y, & Oda K (2005) Using process diagrams for the graphical representation of biological networks. *Nat.Biotechnol.* 23(8):961-966.
22. Sauro HM, *et al.* (2003) Next generation simulation tools: the Systems Biology Workbench and BioSPICE integration. *OMICS.* 7(4):355-372.
23. Akaike H (1974) A new look at the statistical model identification. . *IEEE Trans. Automatic Control* 19(6):716-723.

Fig. S1

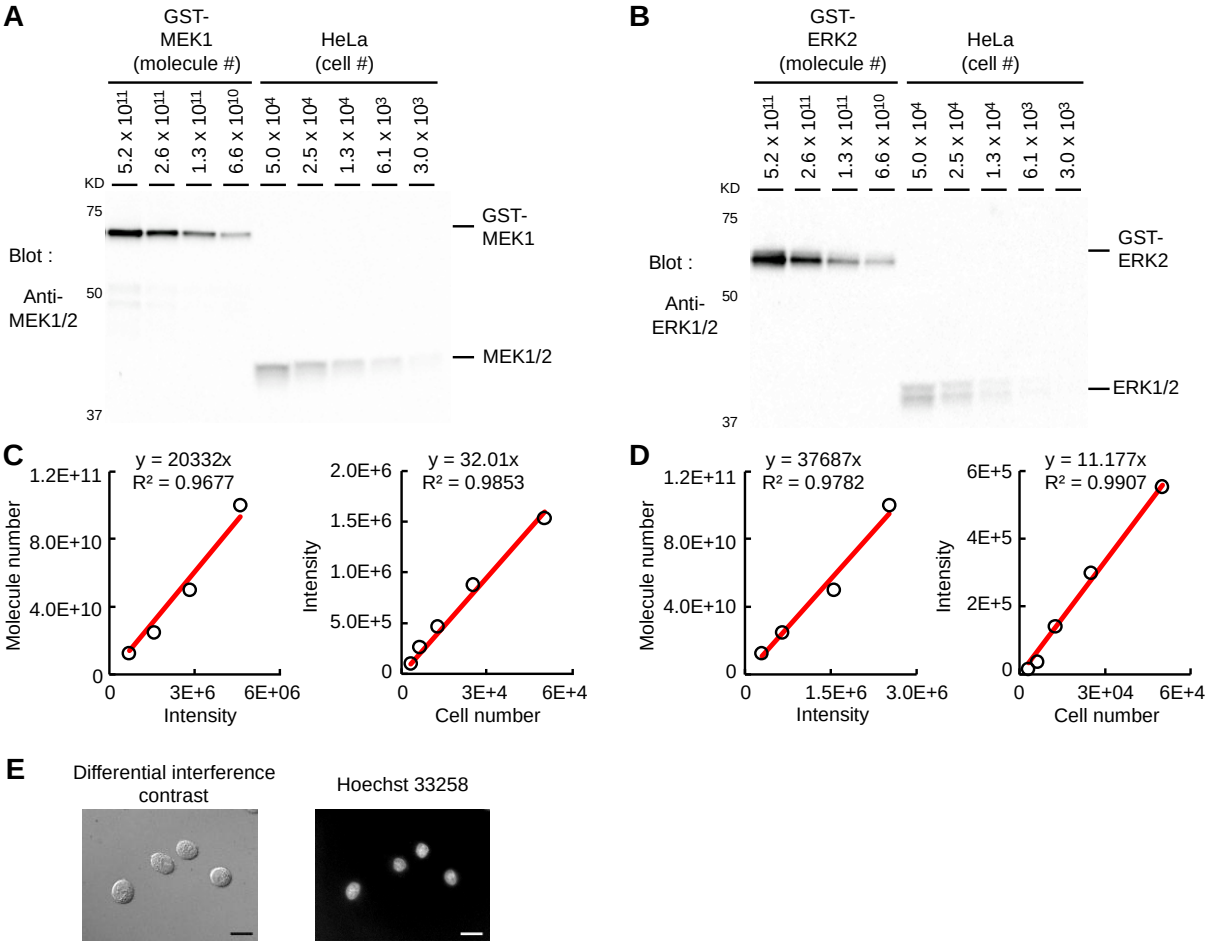

Fig. S1. Quantification of protein concentrations, dissociation constant, and nucleocytoplasmic shuttling rates. (A and B) For the determination of the molecule numbers of MEK and ERK, serial dilution of recombinant GST-tagged proteins and total cell lysates of HeLa cells were separated by SDS-PAGE, followed by immunoblotting with anti-MEK1/2 (A) and anti-ERK1/2 (B) antibodies. The bound antibodies were detected and quantified. (C and D) The bands in A and B were quantified and plotted as scatter plots, showing the linear relation between intensity and dilution of molecules and cell number. (E) For quantification of the volume of the cytoplasm and nucleus, HeLa cells were trypsinized and stained with Höechst 33258. Cells were imaged with differential interference contrast microscopy (upper, cytoplasm and nucleus) or fluorescence microscopy (lower, nucleus).

Fig. S2

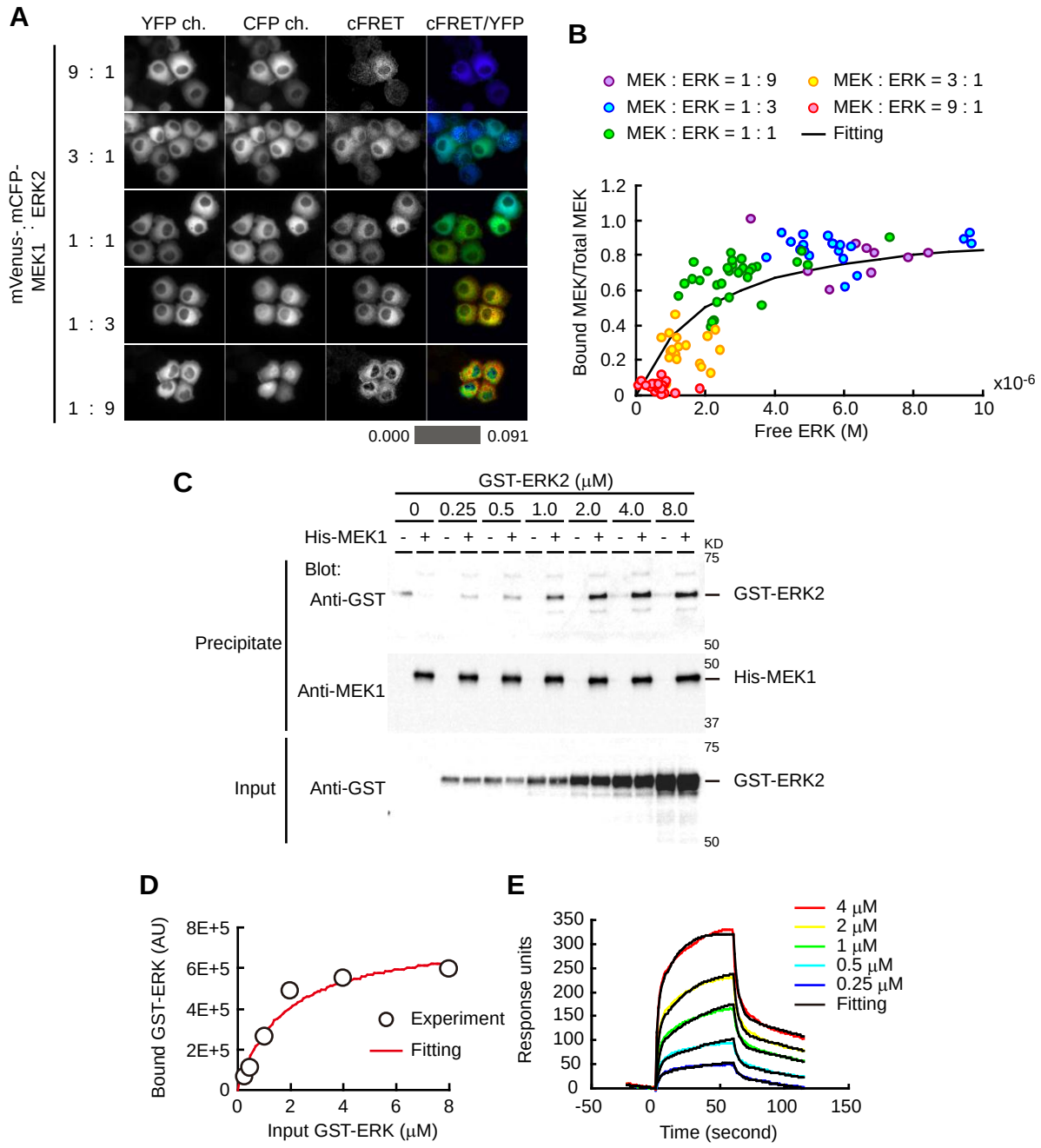

Fig. S2. Measurements of dissociation constant for the binding of MEK and ERK. (A) HeLa cells were transfected with plasmids encoding mVenus-MEK1 and mCFP-ERK2 as indicated ratio. Images of YFP, CFP and FRET were acquired two days after transfection. Then, corrected FRET image (cFRET) images were created by several corrections described in SI Materials and Methods. cFRET/YFP ratio images are shown in the intensity-modulated display mode, in which eight colors from red to blue are used to represent the cFRET/YFP ratio with the intensity of each color indicating the mean intensity of cFRET and YFP. The upper and lower limits of the ratio range are shown in the bottom. (B) Fraction of ERK-bound MEK (Bound MEK/Total MEK) versus the concentration of free ERK in each cell is plotted with the fitted curve. The dissociation constant was calculated as described in SI Materials and Methods. (C) Dissociation constant between MEK and ERK was measured by using in vitro binding assay. (D) The amount of bound versus free ERK is plotted with the fitted curve (Kd is 1.5 x 10^{-6} M). (E) Interaction between MEK and ERK was monitored in real time by surface plasmon resonance spectroscopy analysis. Increasing concentrations of ERK (0.25-4.0 x 10^{-6} M) were passed over a sensor chip with immobilized MEK for 60 s (association phase) before the flow was switched to buffer alone for another 60 s (dissociation phase). Association and dissociation rate constants were derived using BIAevaluation 4.1 software.

Fig. S3

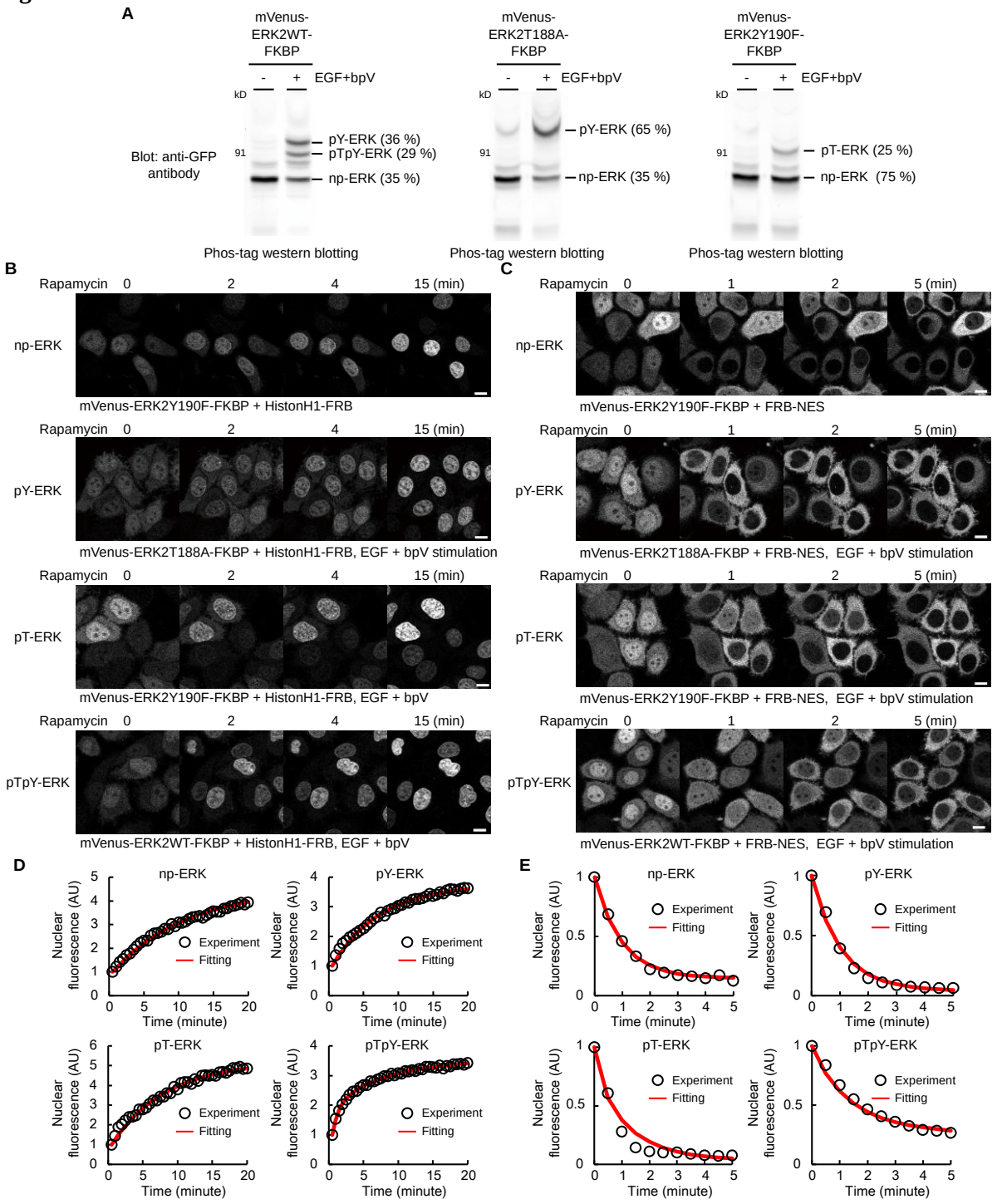

Fig. S3. Measurements of nucleocytoplasmic shuttling rates of phospho-isoforms of ERK. (A) HeLa cells expressing mVenus/FKBP-tagged ERK wild type (WT), T188A, or Y190F were serum-starved for 6-12 h and stimulated with 2.0 x 10^{-6} g/l EGF and 1.0 x 10^{-4} M bpV for 10 min. Cells were lysed and subjected to Phos-tag western blotting with anti-GFP antibody. The four phospho-isoforms of ERK are indicated on the right: np, non-phosphorylated; pT, threonine mono-phosphorylated; pY, tyrosine mono-phosphorylated; pTpY, threonine and tyrosine bis-phosphorylated (see Fig. S4 in detail). (B and C) HeLa cells expressing the proteins indicated at the bottom were stimulated with 2.0 x 10^{-6} g/l EGF and 1.0 x 10^{-4} M bpV for 10 min, followed by the addition of 2.5 x 10^{-7} M Rapamycin to trap the proteins at nucleus (B) or cytoplasm (C). (D and E) After Rapamycin treatment, the nuclear fluorescence intensity was monitored and fitted with single (np-ERK), double (pY-ERK, pT-ERK), or triple (pTpY-ERK) exponential curves. The fraction of each exponential curve was determined from the data shown in A. The nuclear import (D) and export (E) rates of each phospho-isoform was obtained from the time constants of the exponential curves.

Fig. S4

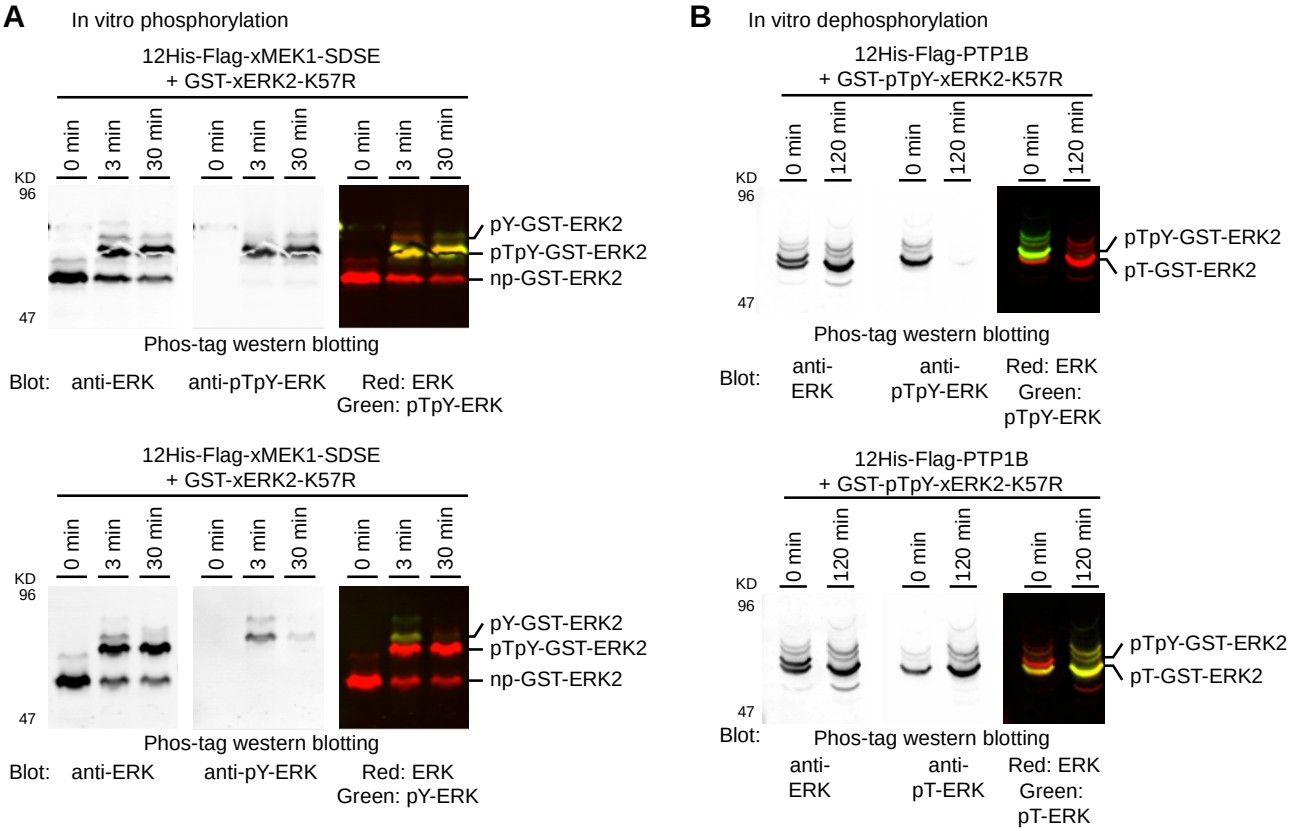

Fig. S4. Separation of phospho-isoforms of ERK by phospho-affinity gel electrophoresis. (A) GST-tagged Xenopus ERK2-KR (K57R, kinase-dead mutant) was phosphorylated in vitro by His-tagged Xenopus MEK1-SDSE (constitutively active mutant) for the indicated periods. Phosphorylated proteins were identified by Phos-tag western blot analysis with anti-ERK1/2 (upper and lower), anti-pTpY-ERK1/2 (upper), and anti-pY-ERK1/2 antibodies (lower). Non-phosphorylated ERK (np-ERK), tyrosine mono-phosphorylated ERK (pY-ERK), and tyrosine and threonine bis-phosphorylated ERK (pTpY-ERK) are denoted on the right. (B) GST-pTpY-ERK2 was dephosphorylated by His-tagged PTP1B to generate pT-ERK2. Phosphorylated proteins were analyzed by using anti-ERK1/2 (upper and lower), anti-pTpY-ERK1/2 (upper), and anti-pT-ERK1/2 antibodies (lower).

Fig. S5

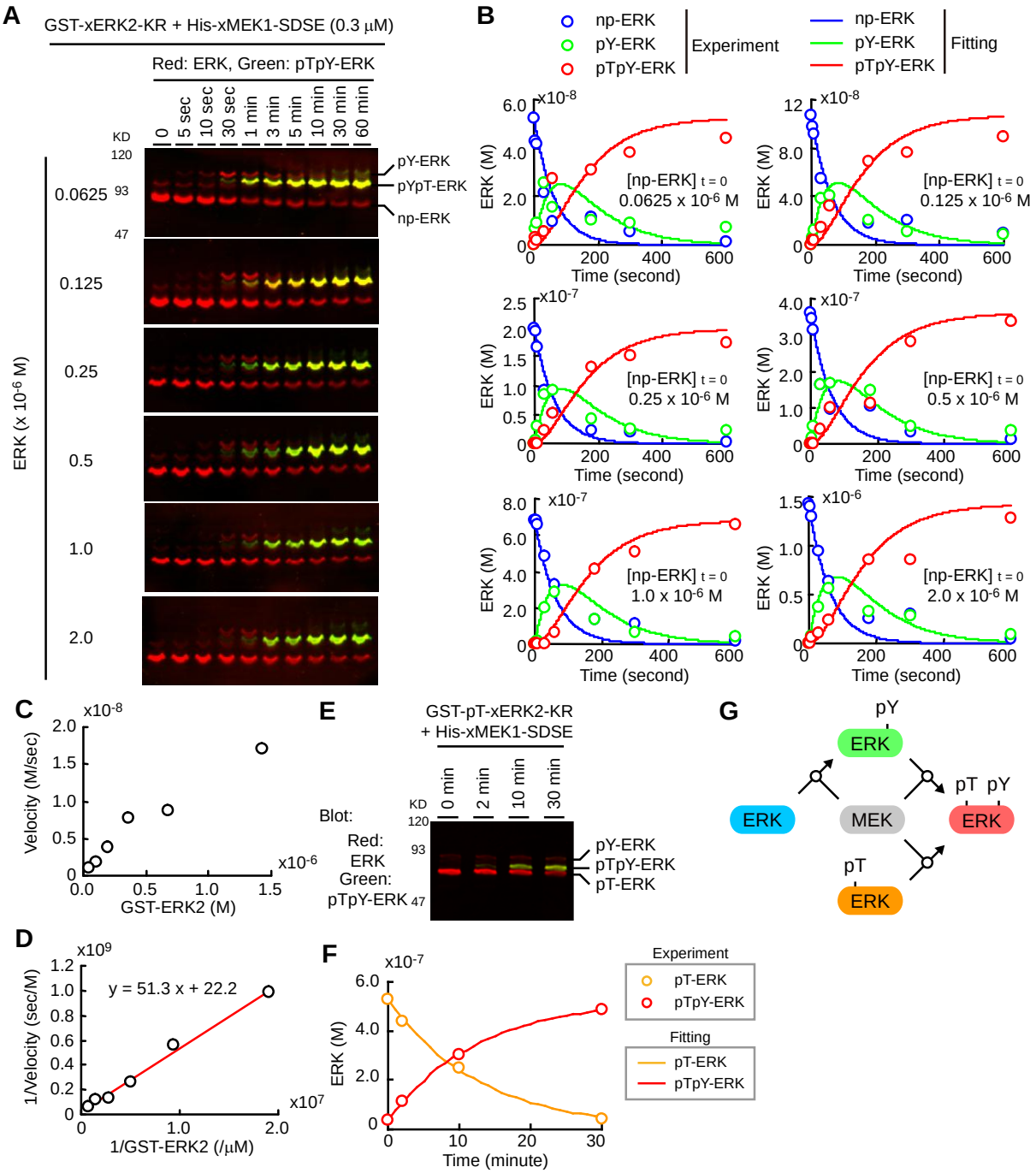

Fig. S5. Measurement of phosphorylation rates *in vitro*. (A) GST-ERK2-KR at the indicated concentrations was phosphorylated by His-tagged MEK1-SDSE (3.0×10^{-7} M) in the presence of 1.0×10^{-3} M ATP for the indicated time period, followed by Phos-tag western blot analysis. Non-phosphorylated ERK (np-ERK), tyrosine mono-phosphorylated ERK (pY-ERK), and tyrosine and threonine bis-phosphorylated ERK (pTpY-ERK) are denoted on the right. (B) The amounts of phospho-isoforms of ERK were quantified by subtracting the amount of non-reactive ERK, and plotted as circles. The data were fitted by a global least-square regression algorithm to a two-steps first-order phosphorylation model to obtain kinetic parameters. (C) The initial velocity of the first phosphorylation step is plotted against the substrate concentration. The velocity is not saturated in up to 1.5×10^{-6} M of substrate, indicating that the Michaelis constant of this phosphorylation step is larger than this range. (D) A Lineweaver-Burk plot of the first phosphorylation step is shown with the linear regression line. (E) GST-pT-ERK2-KR was phosphorylated by His-tagged MEK1-SDSE in the presence of 1.0×10^{-3} M ATP for the indicated period, followed by Phos-tag western blot analysis. (F) The amounts of phospho-isoforms of ERK were quantified and plotted. The data were fitted to a one-step first-order phosphorylation model to obtain kinetic parameters. (G) Schematic diagram of distributive ERK phosphorylation.

Fig. S6

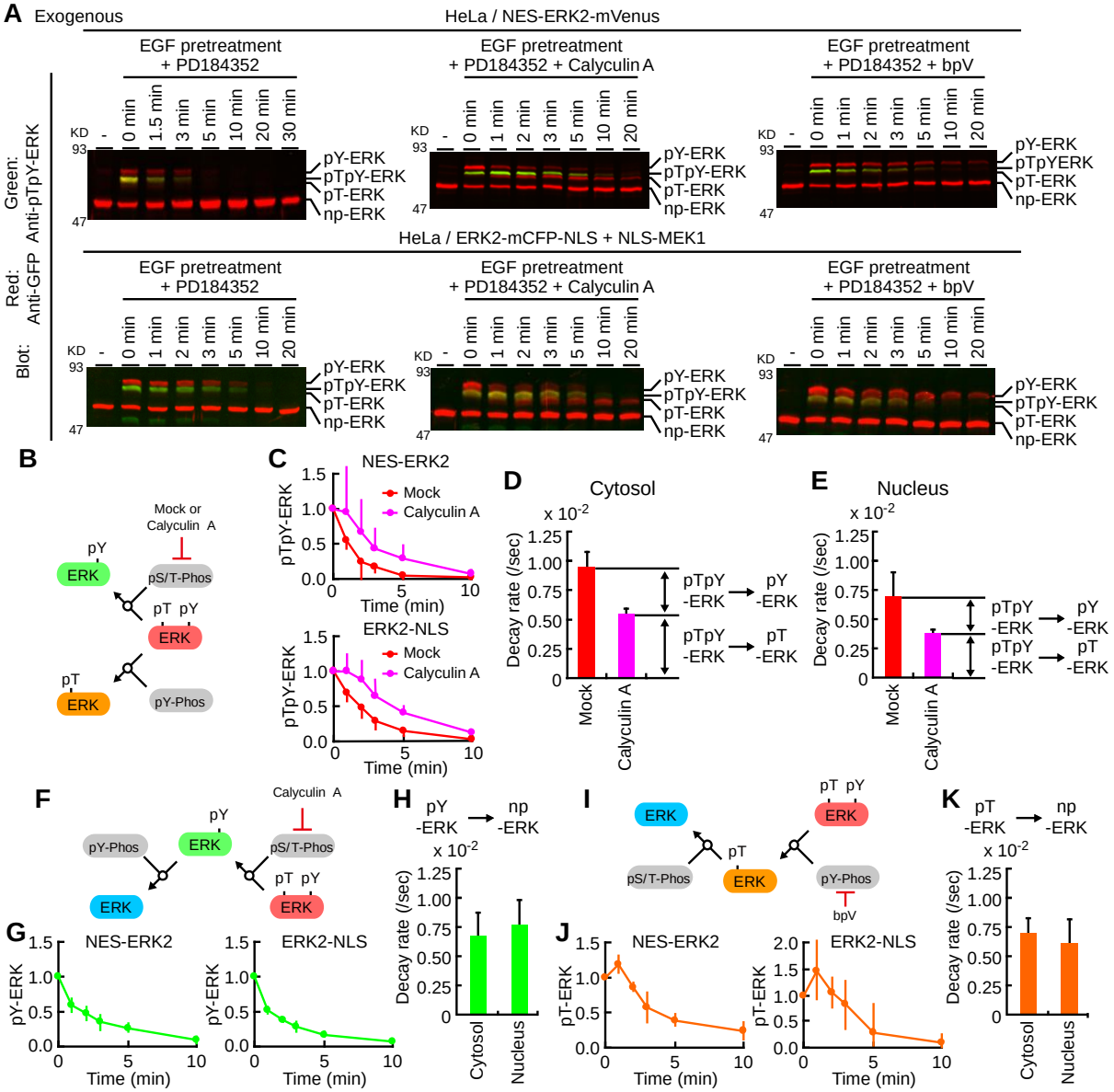

Fig. S6. Measurement of the dephosphorylation rate of ERK. (A) HeLa cells stably expressing NES-ERK2-mVenus (upper) or ERK2-mCFP-NLS with NLS-MEK1 (lower) were serum starved for 12 hours. Cells were left untreated or treated with 1.0 x 10^{-5} g/l EGF for 5 minutes, followed by 1.0 x 10^{-5} M PD184352 with mock (left), 1.0 x 10^{-7} M Calyculin A (center) or 1.0 x 10^{-4} M bpV (right) for the indicated time periods. Cell lysates were subjected to Phos-tag western blot analysis using anti-GFP and anti-pTpY-ERK antibodies. We repeated the same experiments four times with reproducible results, and representative results are shown. (B) Scheme of two dephosphorylation pathways for pTpY-ERK. (C) The decrease of pTpY-ERK after MEK inhibition by PD184352 in the presence or absence of Calyculin A was monitored in cytosol (upper) and nucleus (lower). Bars are SD (n = 4). (E and F) The dephosphorylation rates [/sec] in cytosol (D) and nucleus (E) were measured by fitting the time course of pTpY-ERK decay shown in C with an exponential decay function. Dephosphorylation rates from pTpY-ERK to pT-ERK were simply interpreted as the decay rates with Calyculin A. Dephosphorylation rates from pTpY-ERK to pY-ERK were obtained by subtracting total dephosphorylation rates from those of pTpY-ERK to pT-ERK. (F) Scheme of dephosphorylation pathways for pY-ERK. Calyculin A prevents an influx of pY-ERK via pTpY-ERK. (G) The decrease of pY-ERK upon MEK inhibition by PD184352 in the presence of Calyculin A was monitored in cytosol (left) and nucleus (right). Bars are SD (n = 4). (H) The dephosphorylation rates [/sec] in cytosol and nucleus were measured by fitting the time course of pY-ERK decay with an exponential function. (I) Scheme of dephosphorylation pathways for pT-ERK. bpV prevents an influx of pT-ERK via pTpY-ERK. (J) The decrease of pT-ERK upon MEK inhibition by PD184352 in the presence of bpV was monitored in cytosol (left) and nucleus (right). Bars are SD (n = 4). (K) The dephosphorylation rates [/sec] in cytosol and nucleus were measured by fitting the time course of pT-ERK decay with an exponential function. See SI Text in more details.

Fig. S7

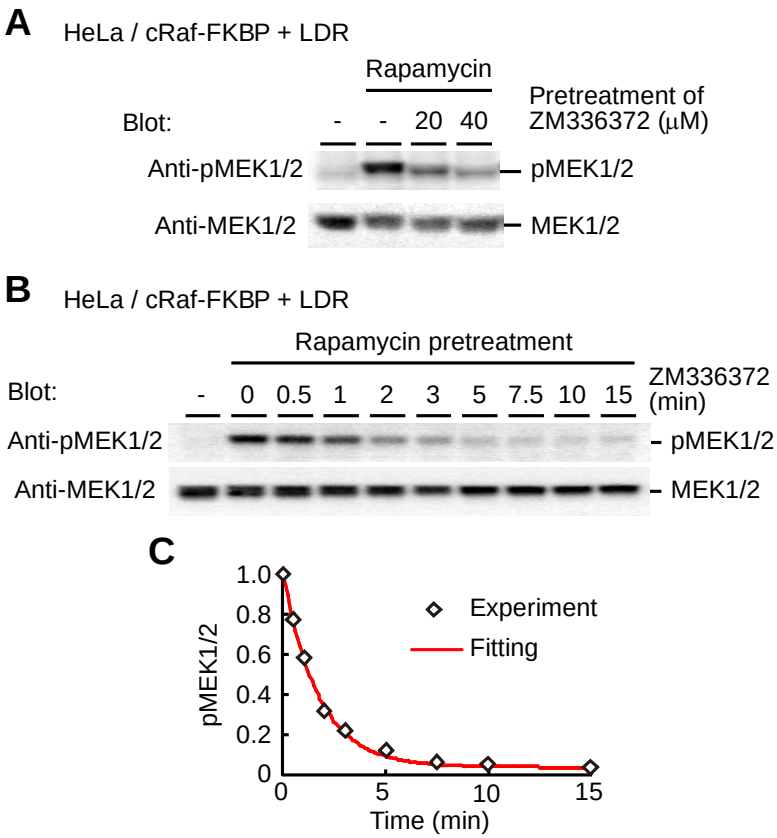

Fig. S7. Measurement of the dephosphorylation rate of MEK. To measure the MEK dephosphorylation rate in HeLa cells, we generated a HeLa cell line stably expressing cRaf-FKBP and LDR. Upon Rapamycin treatment of this cell line, cRaf-FKBP is recruited to plasma membrane and activated rapidly. Consequently, MEK is phosphorylated by the cRaf-FKBP without any perturbations of other signaling pathways. (A) The HeLa cells were left untreated or pretreated with a cRaf inhibitor, ZM336372, for 10 min, and then stimulated with Rapamycin for 30 min. The cell lysates were subjected to SDS PAGE and analyzed by anti-phospho-MEK1/2 (upper) and anti-MEK1/2 (lower) antibodies. (B and C) Measurement of the dephosphorylation rate of MEK. (B) The aforementioned HeLa cells were treated with or without Rapamycin for 15 min, and then treated with ZM336372 for the indicated time period. The cell lysates were collected and subjected to SDS-PAGE followed by immunoblotting analysis with anti-phospho-MEK1/2 (upper) and anti-MEK1/2 (lower) antibodies. These experiments were repeated three times and representative results are shown. (C) The relative amount of phosphorylated MEK1/2 was measured and plotted as a function of time after ZM336372 addition (min). The decay of MEK is fitted to the red line with a single exponential decay function.

Fig. S8

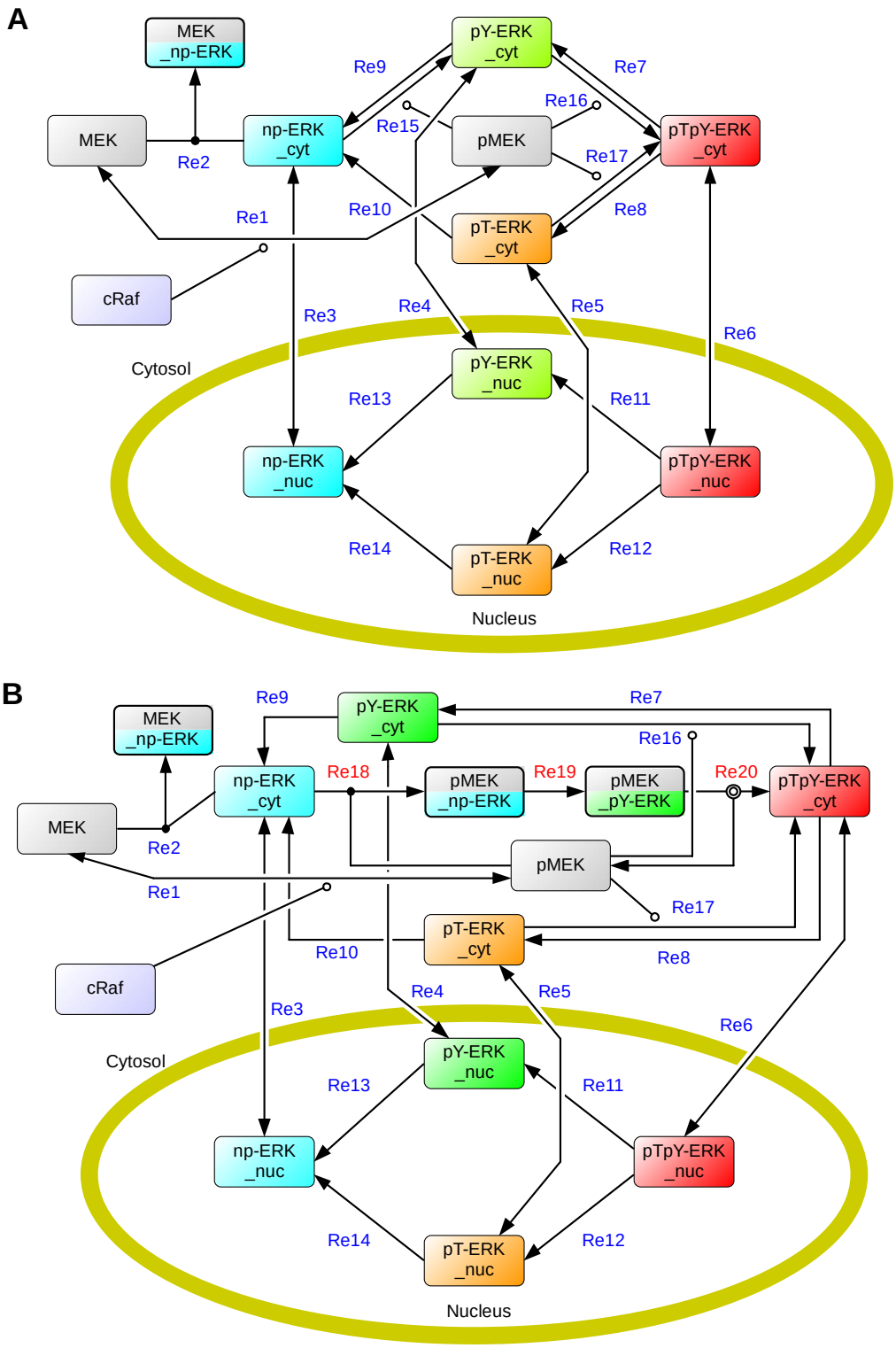

Fig. S8. Diagram of the distributive and processive model. (A) A process diagram of the distributive phosphorylation model of the MEK-ERK module was represented. The arrows represent the reactions (Re), which are numbered from 1 to 17 as described in the Table S2. (B) A process diagram of the processive phosphorylation model of the MEK-ERK module. The arrows represent the reactions (Re), which are numbered from 1 to 20 as described in the Table S2. Blue numbers are common between the distributive model and the processive model. Red numbers are reactions specific to the processive model.

Fig. S9

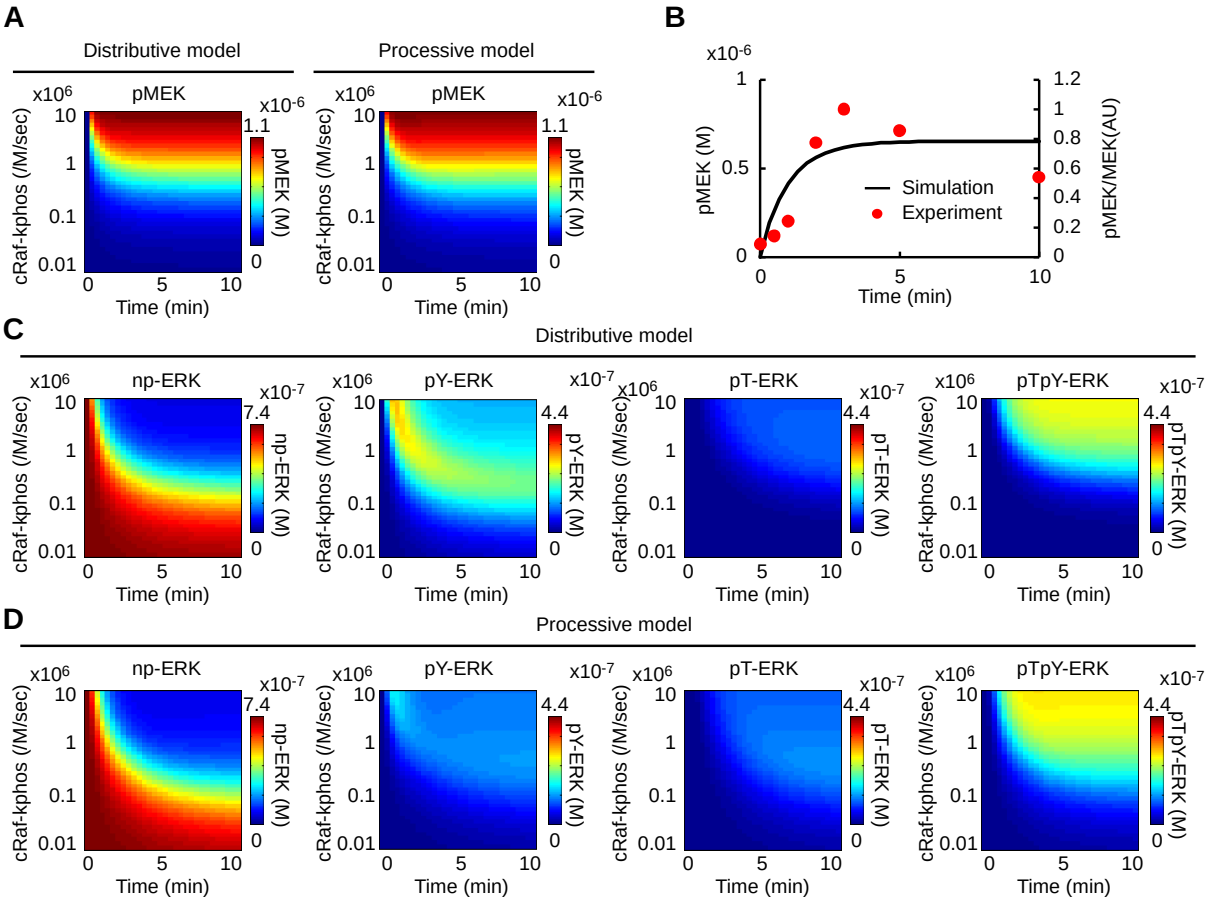

Fig. S9. Dynamics of ERK phosphorylation with varying MEK activity. Experimentally-determined parameters were used for the numerical simulations based on the distributive model and processive model. (A) Heat maps of the concentration of phosphorylated MEK upon stimulation in distributive model (left) and processive model (right). Horizontal and vertical axes indicate time after stimulation (minute) and kcat/Km value (Raf_kphos) of cRaf kinase for MEK phosphorylation as an input strength, respectively. (B) HeLa cells were stimulated with 1.0 x 10^{-5} g/l EGF, and lysed with SDS sample buffer at the indicated time points. The cell lysates were subjected to Western blotting analysis with anti-MEK1/2 and anti-phospho-MEK1/2 antibodies. The ratio of phospho-MEK to MEK (pMEK/MEK) is plotted against the time after EGF stimulation (red circle). In addition, the time course of MEK phosphorylation in the distributive model at kcat/Km value of 1.0 x 10^{6} [/M/sec] is superimposed in the same figure. (C and D) Shown here are the heat maps of the concentration of the indicated phospho-isoforms of ERK upon stimulation in the distributive model (C) and processive model (D).

Fig. S10

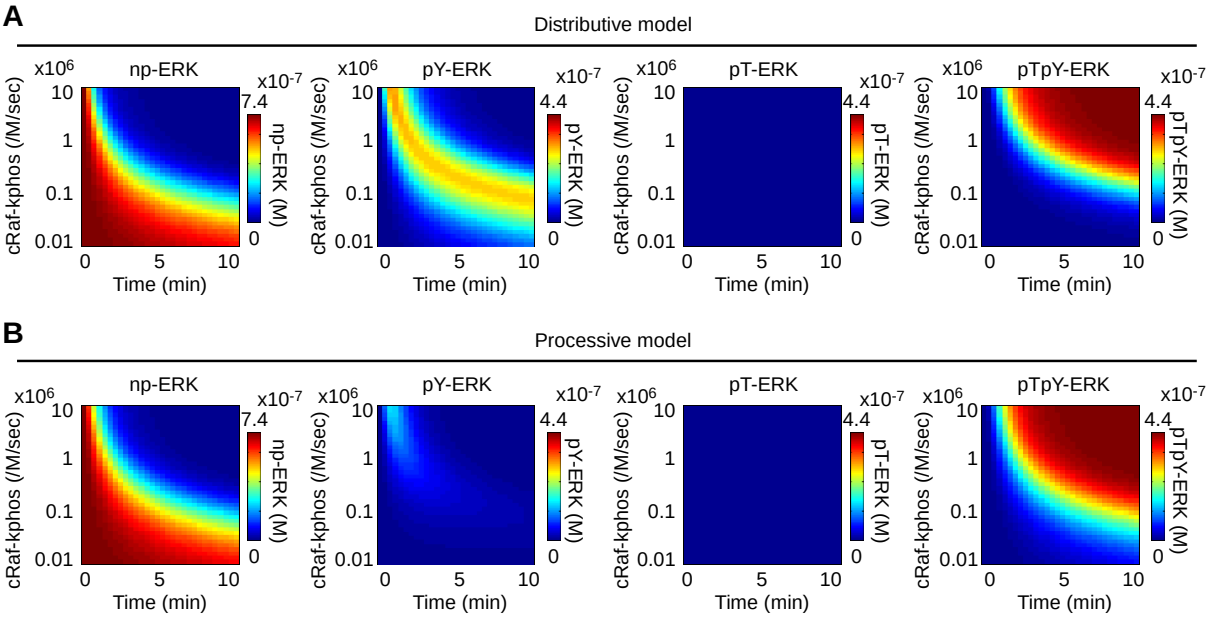

Fig. S10. Dynamics of ERK phosphorylation in the absence of dephosphorylation pathways. Shown here are heat maps of concentration of the indicated phospho-isoforms of ERK upon stimulation in the distributive model (A) and processive model (D) as well as shown in Figure S9 except for the lack of dephosphorylation pathways.

Fig. S11

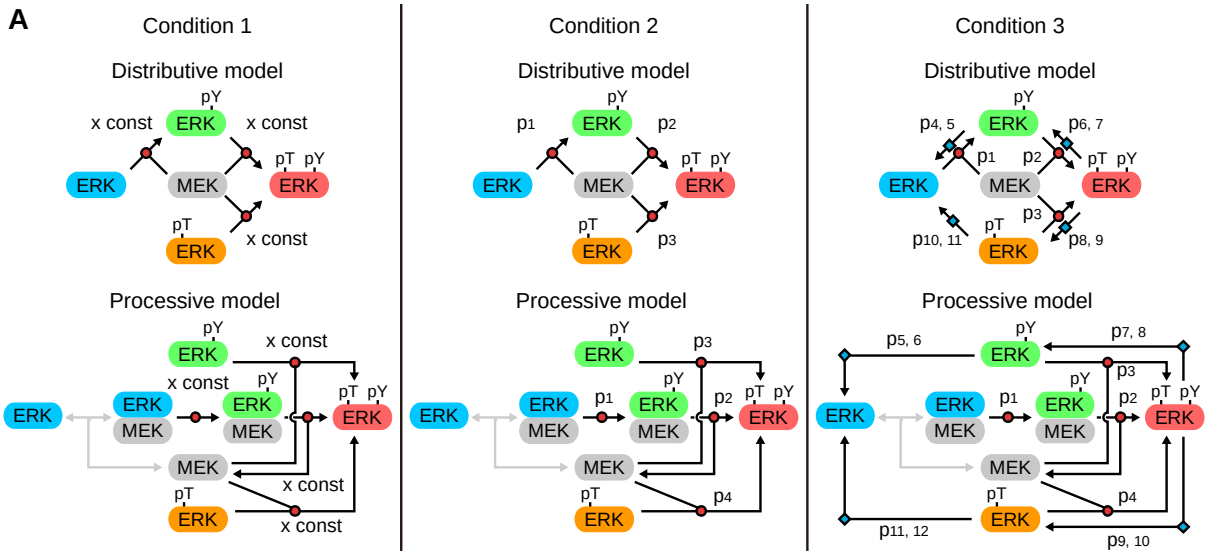

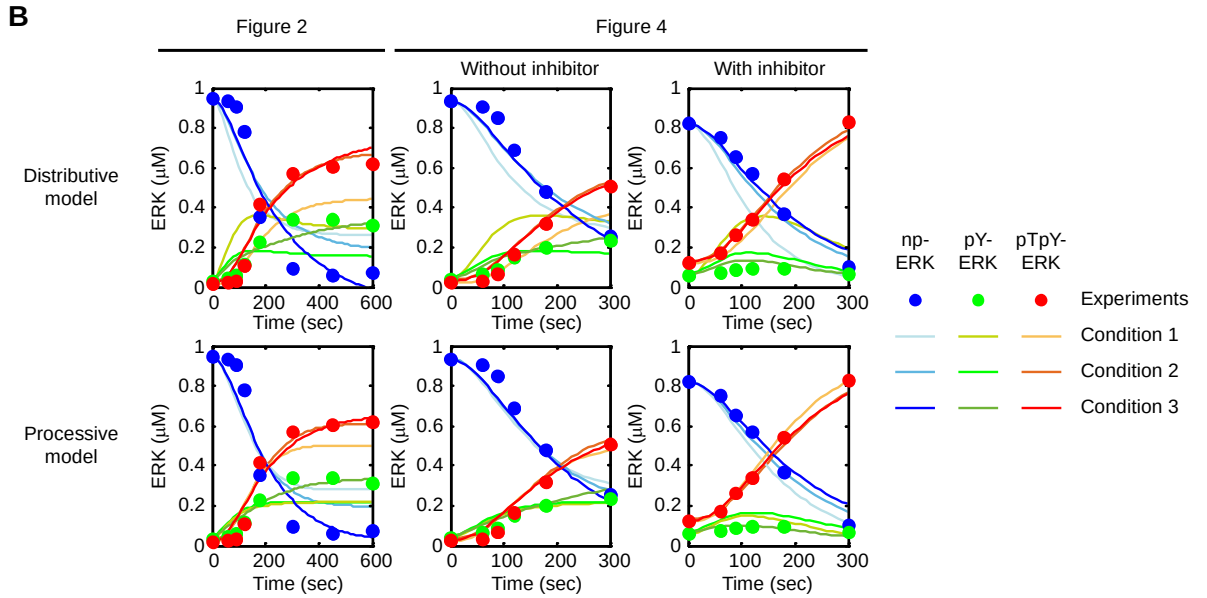

C

	Distributive model				Processive model			
	RSS	AIC	nH	Variables	RSS	AIC	nH	Variables
Condition 1	1.165	-36.3	1.66	1	0.421	-51.6	1.12	1
Condition 2	0.382	-49.0	1.79	3	0.275	-52.0	1.13	4
Condition 3	0.204	-42.5	2.27	11	0.180	-42.3	1.42	12

Fig. S11. Numerical validation of the processive phosphorylation model. (A) Numerical validation of the phosphorylation models by parameter fittings. (A) The conditions for the parameter fittings are illustrated. Black lines represent reactions to be optimized by parameter search. Condition 1 (left) aims to fit the data (Fig. 2E and Fig. 4D) by optimizing the quantity of the activated MEK; therefore the models have only 1 degree of freedom. Condition 2 (middle) aims to fit the data by independently changing the MEK activities against np-ERK, pY-ERK, and pT-ERK, allowing 3 and 4 degrees of freedom in the distributive and processive models, respectively. Condition 3 (right) aims to fit the data by changing all phosphorylation and dephosphorylation rates, allowing 11 and 12 degrees of freedom in the distributive and processive models, respectively. (B) The results of curve fitting are shown with the experimental data in Fig. 2E and Fig. 4D. (C) A table presents a summary of the parameter fitting. RSS, AIC, and nH refer to residual sum of square, Akaike information criterion, and Hill coefficient, respectively. Based on the AIC and Hill coefficient values, the processive model in Condition 2 is the most plausible model. In Condition 3, even though the AIC value of the distributive model is comparable to that of the processive model, the AIC value is much larger than that obtained for the processive model in Condition 2, suggesting over-fitting.

Fig. S12

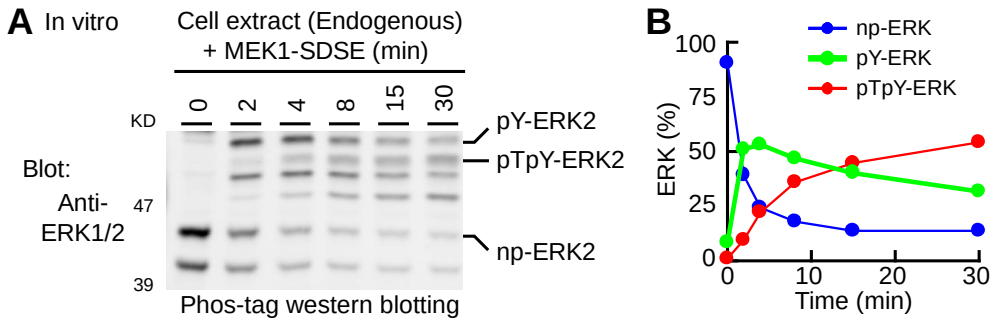

Fig. S12. In vitro ERK phosphorylation by using cell extract. Cytoplasmic extract prepared from HEK-293F cells were diluted with in vitro kinase buffer containing ATP and constitutively active MEK, and incubated for the indicated period (min). (A) The reaction solution were subjected to Phos-tag western blotting analysis. (B) The fractions of np-ERK2 (blue), pY-ERK2 (green), and pTpY-ERK2 (red) are plotted against time.

Fig. S13

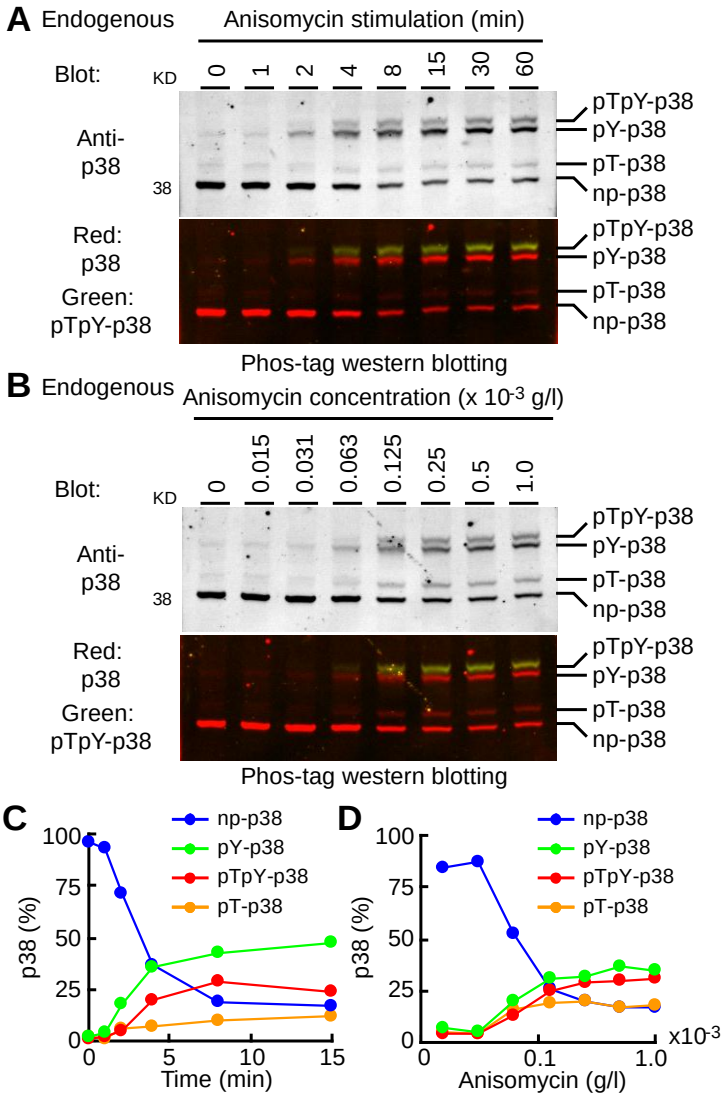

Fig. S13. Processive phosphorylation of p38 MAP kinase. (A) HeLa cells were stimulated with 1.0 x 10^{-3} g/l anisomycin at the indicated time. Cell lysates were subjected to Phos-tag western blot analysis. (B) HeLa cells were stimulated with indicated concentration of anisomycin for 30 min. Cell lysates were subjected to Phos-tag western blot analysis. (C and D) The phospho-isoforms of p38 in A and B were quantified and plotted. Notably, preceding accumulation of pY-p38, which was typical hallmark of distributive phosphorylation, was not observed in time-course (C) and steady-state (D) analysis.

Fig. S14

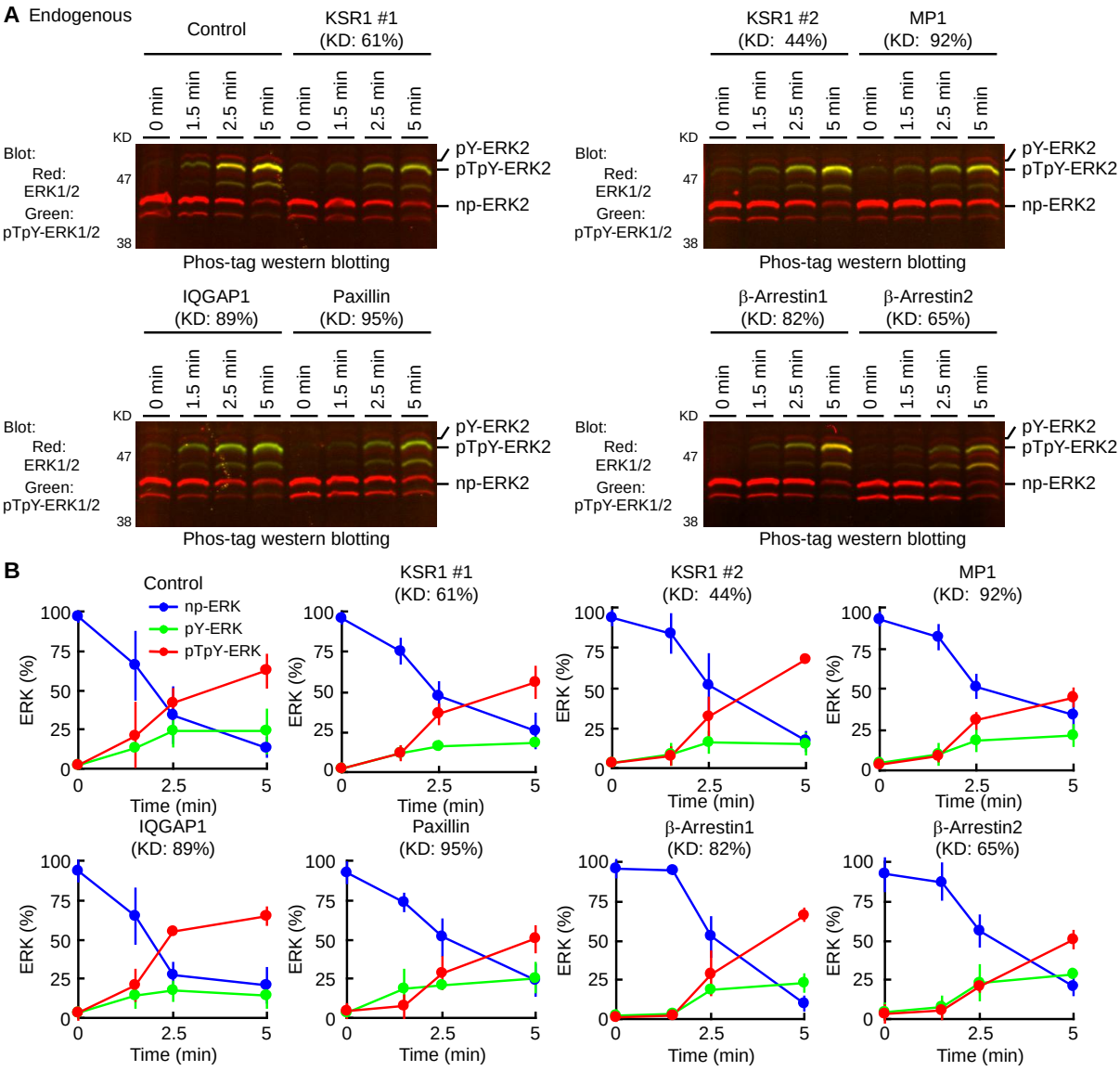

Fig. S14. Effects of scaffold proteins on the mode of ERK phosphorylation. (A) HeLa cells were transfected with siRNA for control or scaffold proteins as indicated. Three days after transfection, the HeLa cells were stimulated with 1.0 x 10^{-5} g/l EGF and analyzed at the indicated time. Cells were subjected to Phos-tag western blot analysis. Knockdown efficiency (KD, %) of siRNA was determined by quantitative RT-PCR analysis. (B) The phospho-isoforms of ERK quantified in A are plotted with SD (n = 3). See SI Text in more details.

Table S1

Table S1. Concentration of cRaf, MEK, and ERK in a HeLa cell.

Species	Concentration (M)			Comment
	Average	SD	N	
cRaf	1.3×10^{-8}	-	-	Fujioka et al. JBC 2006
MEK	1.2×10^{-6}	5.2×10^{-7}	3	Fig. S1
ERK	7.4×10^{-7}	3.3×10^{-7}	3	Fig. S1

Parameter	Volume (l)			Comment
	Average	SD	N	
Cytoplasm	2.8×10^{-12}	7.6×10^{-13}	20	Fig. S1
Nucleus	6.0×10^{-13}	2.1×10^{-13}	20	Fig. S1

MEK and ERK mean the total concentration of both MEK1 and MEK2 and both ERK1 and ERK2, respectively.

Table S2

Table S2. Kinetic models and parameters.

Reaction #	Reaction	Parameters					Comments
			Average	SD	Unit	N	
Re1	MEK + **cRaf** <=> pMEK	kf	1.0×10^{6}	-	/M/sec	-	Arbitrary
		kb	9.6×10^{-3}	2.2×10^{-3}	/sec	3	Fig. S7
Re2	MEK + np-ERK_cyt <=> MEK_np-ERK	kf	1.8×10^{5}	-	/M/sec	1	Fig. S2E[1]
		kb	2.7×10^{-1}	-	/sec	1	
Re3	np-ERK_cyt <=> np-ERK_nuc	kf	1.7×10^{-3}	5.5×10^{-4}	/sec	17	Fig. S3
		kb	1.3×10^{-2}	3.5×10^{-3}	/sec	7	Fig. S3
Re4	pY-ERK_cyt <=> pY-ERK_nuc	kf	2.5×10^{-3}	7.9×10^{-4}	/sec	19	Fig. S3
		kb	1.7×10^{-2}	4.6×10^{-3}	/sec	10	Fig. S3
Re5	pT-ERK_cyt <=> pT-ERK_nuc	kf	2.2×10^{-3}	9.9×10^{-4}	/sec	16	Fig. S3
		kb	4.9×10^{-2}	2.0×10^{-2}	/sec	7	Fig. S3
Re6	pTpY-ERK_cyt <=> pTpY-ERK_nuc	kf	8.2×10^{-3}	5.7×10^{-3}	/sec	15	Fig. S3
		kb	7.6×10^{-3}	3.6×10^{-3}	/sec	16	Fig. S3
Re7	pTpY-ERK_cyt -> pY-ERK_cyt	kf	4.0×10^{-3}	8.5×10^{-4}	/sec	4	Fig. S6
Re8	pTpY-ERK_cyt -> pT-ERK_cyt	kf	5.5×10^{-3}	4.7×10^{-4}	/sec	4	Fig. S6
Re9	pY-ERK_cyt -> np-ERK_cyt	kf	6.7×10^{-3}	2.0×10^{-3}	/sec	4	Fig. S6
Re10	pT-ERK_cyt -> np-ERK_cyt	kf	6.8×10^{-3}	1.1×10^{-3}	/sec	4	Fig. S6
Re11	pTpY-ERK_nuc -> pY-ERK_nuc	kf	3.2×10^{-3}	1.7×10^{-3}	/sec	4	Fig. S6
Re12	pTpY-ERK_nuc -> pT-ERK_nuc	kf	3.8×10^{-3}	3.0×10^{-4}	/sec	4	Fig. S6
Re13	pY-ERK_nuc -> np-ERK_nuc	kf	7.7×10^{-3}	2.1×10^{-3}	/sec	4	Fig. S6
Re14	pT-ERK_nuc -> np-ERK_nuc	kf	5.8×10^{-3}	2.2×10^{-3}	/sec	4	Fig. S6
Re15	np-ERK_cyt + **pMEK** -> pY-ERK_cyt	kf	3.9×10^{4}	1.9×10^{4}	/M/sec	2	Fig. S5[2]
Re16	pY-ERK_cyt + **pMEK** -> pTpY-ERK_cyt	kf	2.1×10^{4}	1.1×10^{4}	/M/sec	2	Fig. S5[2]
Re17	pT-ERK_cyt + **pMEK** -> pTpY-ERK_cyt	kf	2.0×10^{4}	-	/M/sec	1	Fig. S5
Re18	pMEK + np-ERK_cyt <=> pMEK_np-ERK	kf	1.8×10^{5}	-	/M/sec	-	Assumption[3]
		kb	2.7×10^{-1}	-	/sec	-	
Re19	pMEK_np-ERK -> pMEK_pY-ERK	kf	7.3×10^{-2}	- -	/sec	-	Calculated from Re15 and Re 18[4]
Re20	pMEK_pY-ERK -> pTpY-ERK_cyt + pMEK	kf	5.0×10^{-2}	-	/sec	-	Estimated from Figure 2E

The reaction number is indicated in Figure S8A and S8B. Bold character means enzyme. The symbols <=> and -> indicate a reversible reaction and an irreversible reaction, respectively. kf and kb are forward and reverse kinetic parameters, respectively.

[1] kf and kb are obtained by Biacore with 5 different sets of ligand concentration. Dissociation constants, which are measured by FRET and in vitro binding assay, are 1.7 x 10^-6 ± 6.8 x 10 ^-7 [M] (N = 3) (Fig. S2A and B) and 1.8 x 10^-6 [M] (N = 1) (Fig. S2C and D), respectively.

[2] Parameters are obtained by global fitting of 2 independent experiments with 10 different sets of substrate and enzyme concentration.

[3] Assuming that the association/dissociation rate constants of the binding bewtween pMEK and ERK are comparable with them of the binding of MEK and ERK.

[4] kcat/Km = kcat/(kb+kcat)/kf, and then 0.038 = kcat/(0.27+kcat)/1.8. Thus, kcat = 0.79.

Table S3

Table S3. Summary of parameters fitted with three different conditions in Figure S11.

Reaction #	Reaction	Initial value (Unit)			Fitting condition 1		Fitting condition 2		Fitting condition 3	
					Distributive	Processive	Distributive	Processive	Distributive	Processive
Re7	pTpY-ERK_cyt -> pY-ERK_cyt	kf	4.0×10^{-3}	/sec					6.5×10^{-3}	9.2×10^{-3}
Re8	pTpY-ERK_cyt -> pT-ERK_cyt	kf	5.5×10^{-3}	/sec					-6.1×10^{-3}	-3.0×10^{-4}
Re9	pY-ERK_cyt -> np-ERK_cyt	kf	6.7×10^{-3}	/sec					6.8×10^{-3}	-1.2×10^{-3}
Re10	pT-ERK_cyt -> np-ERK_cyt	kf	6.8×10^{-3}	/sec					7.7×10^{-3}	1.0×10^{-3}
Re11	pTpY-ERK_nuc -> pY-ERK_nuc	kf	3.2×10^{-3}	/sec					1.0×10^{-3}	2.8×10^{-3}
Re12	pTpY-ERK_nuc -> pT-ERK_nuc	kf	3.8×10^{-3}	/sec					8.6×10^{-3}	-2.3×10^{-3}
Re13	pY-ERK_nuc -> np-ERK_nuc	kf	7.7×10^{-3}	/sec					-4.5×10^{-3}	7.8×10^{-3}
Re14	pT-ERK_nuc -> np-ERK_nuc	kf	5.8×10^{-3}	/sec					1.7×10^{-3}	6.9×10^{-3}
Re15	np-ERK_cyt +**pMEK** -> pY-ERK_cyt	kf	3.9×10^{4}	/M/sec	2.9×10^{4}		1.7×10^{4}		1.4×10^{4}	
Re16	pY-ERK_cyt +**pMEK** -> pTpY-ERK_cyt	kf	2.1×10^{4}	/M/sec	1.6×10^{4}	1.3×10^{4}	3.9×10^{4}	1.6×10^{4}	4.6×10^{4}	2.0×10^{4}
Re17	pT-ERK_cyt +**pMEK** -> pTpY-ERK_cyt	kf	2.0×10^{4}	/M/sec	1.4×10^{4}	1.2×10^{4}	2.8×10^{7}	3.6×10^{7}	2.3×10^{4}	3.3×10^{4}
Re19	pMEK_np-ERK -> pMEK_pY-ERK	kf	7.9×10^{-2}	/sec		4.7×10^{-2}		3.9×10^{-2}		3.2×10^{-2}
Re20	pMEK_pY-ERK -> pTpY-ERK_cyt + pMEK	kf	5×10^{-2}	/sec		3.0×10^{-2}		2.3×10^{-2}		4.2×10^{-2}

The reaction number is indicated in Figure S8A and S8B. Bold character means enzyme. The symbols <=> and -> indicate a reversible reaction and an irreversible reaction, respectively. kf and kb are forward and reverse kinetic parameters, respectively.